SIAM J. SCI. COMPUT.
Vol. 37, No. 2, pp. B305–B331

LINEARLY IMPLICIT IMEX RUNGE–KUTTA METHODS FOR A CLASS OF DEGENERATE CONVECTION-DIFFUSION PROBLEMS*

SEBASTIANO BOSCARINO†, RAIMUND BÜRGER‡, PEP MULET§, GIOVANNI RUSSO†, AND LUIS M. VILLADA¶

Abstract. Multispecies kinematic flow models with strongly degenerate diffusive corrections give rise to systems of nonlinear convection-diffusion equations of arbitrary size. Applications of these systems include models of polydisperse sedimentation and multiclass traffic flow. Implicit-explicit (IMEX) Runge–Kutta (RK) methods are suitable for the solution of these convection-diffusion problems since the stability restrictions, coming from the explicitly treated convective part, are much less severe than those that would be deduced from an explicit treatment of the diffusive term. These schemes usually combine an explicit RK scheme for the time integration of the convective part with a diagonally implicit one for the diffusive part. In [R. Bürger, P. Mulet, and L. M. Villada, *SIAM J. Sci. Comput.*, 35 (2013), pp. B751–B777] a scheme of this type is proposed, where the nonlinear and nonsmooth systems of algebraic equations arising in the implicit treatment of the degenerate diffusive part are solved by smoothing of the diffusion coefficients combined with a Newton–Raphson method with line search. This nonlinearly implicit method is robust but associated with considerable effort of implementation and possibly CPU time. To overcome these shortcomings while keeping the advantageous stability properties of IMEX-RK methods, a second variant of these methods is proposed in which the diffusion terms are discretized in a way that more carefully distinguishes between stiff and nonstiff dependence, such that in each time step only a linear system needs to be solved still maintaining high order accuracy in time, which makes these methods much simpler to implement. In a series of examples of polydisperse sedimentation and multiclass traffic flow, it is demonstrated that these new linearly implicit IMEX-RK schemes approximate the same solutions as the nonlinearly implicit versions, and in many cases these schemes are more efficient.

Key words. implicit-explicit Runge–Kutta schemes, degenerate convection-diffusion equations, linearly implicit methods, polydisperse sedimentation, multiclass traffic flow

AMS subject classifications. 65M20, 65L04, 65L06, 35L65, 76T20

DOI. 10.1137/140967544

*Submitted to the journal's Computational Methods in Science and Engineering section May 2, 2014; accepted for publication (in revised form) February 17, 2015; published electronically April 14, 2015.

http://www.siam.org/journals/sisc/37-2/96754.html

†Department of Mathematics and Computer Science, University of Catania, 95125 Catania, Italy (boscarino@dmi.unict.it, russo@dmi.unict.it). The work of the these authors was partially supported by project PRIN 2009, "Innovative Numerical Methods of Hyperbolic Problems with Applications to Fluid Dynamics, Kinetic Theory and Computational Biology," Protocol 2009588FHJ, of the Italian Ministry of Education, University and Research.

‡CI^{2}MA and Departamento de Ingeniería Matemática, Facultad de Ciencias Físicas y Matemáticas, Universidad de Concepción, Casilla 160-C, Concepción, Chile (rburger@ing-mat.udec.cl). This author's work was supported by Fondecyt project 1130154; BASAL project CMM, Universidad de Chile and Centro de Investigación en Ingeniería Matemática (CI^{2}MA), Universidad de Concepción; Conicyt project Anillo ACT1118 (ANANUM); Red Doctoral REDOC.CTA, MINEDUC project UCO1202; and CRHIAM project CONICYT/FONDAP/15130015.

§Departament de Matemàtica Aplicada, Universitat de València, Av. Dr. Moliner 50, E-46100 Burjassot, Spain (mulet@uv.es). This author's work was partially supported by Spanish MINECO project MTM2011-22741.

¶Departamento de Matemática, Facultad de Ciencias, Universidad del Bío-Bío, Casilla 5-C, Concepción, Chile (lvillada@ubiobio.cl). This author's work was supported by Fondecyt project 11140708.

1. Introduction.

1.1. Scope. This paper is concerned with numerical methods for systems of nonlinear convection-diffusion equations of the type

$$\partial_t \Phi + \partial_x \boldsymbol{f}(\Phi) = \partial_x \big(\boldsymbol{B}(\Phi) \partial_x \Phi \big), \tag{1.1}$$

where $\Phi = (\phi_1, \ldots, \phi_N)^{\mathrm{T}}$ is the desired solution as a function of spatial position x and time t, $\boldsymbol{f}(\Phi) = (f_1(\Phi), \ldots, f_N(\Phi))^{\mathrm{T}}$ is a vector of flux density functions, and $\boldsymbol{B}(\Phi)$ is a given $N \times N$ matrix function expressing a diffusive correction, where we allow that $\boldsymbol{B}(\Phi) = \boldsymbol{0}$ on a set of nonzero N-dimensional measure, so that (1.1) is possibly strongly degenerate. The system (1.1) is supplied with an initial condition and zero-flux or periodic boundary conditions. We focus on two applications, namely, a model of polydisperse sedimentation where the diffusive correction accounts for sediment compressibility [3], and a version of the multiclass Lighthill–Whitham–Richards (MCLWR) traffic model [2, 28] where the diffusive correction describes the effects of reaction times and anticipation lengths.

An implicit treatment of the diffusion terms can overcome the drastic time step size restrictions imposed by the stability condition for explicit schemes applied to parabolic equations. This idea was used in [10] to introduce semi-implicit, so-called implicit-explicit (IMEX) Runge–Kutta (RK) schemes for (1.1), which involve the solution of highly nonlinear and nonsmooth systems of algebraic equations. This is achieved in [10] by a regularization of the nonsmooth diffusion coefficients combined with a suitable solver for the resulting nonlinear systems in an efficient way. While these techniques turned out to be robust and provide approximate solutions even when simpler methods (e.g., the Newton–Raphson (NR) method without line search) do not converge, their effort of implementation is considerable.

It is the purpose of this work to propose a new class of semi-implicit methods for the solution of (1.1) (see [5]) which are strongly inspired by partitioned RK methods [16]. To describe the main idea, assume that the semidiscrete formulation of (1.1) can be written in vector form as

$$\frac{\mathrm{d}\boldsymbol{\Phi}}{\mathrm{d}t} = -\frac{1}{\Delta x}(\Delta^- \boldsymbol{f})(\boldsymbol{\Phi}) + \frac{1}{\Delta x^2} \boldsymbol{\mathcal{B}}(\boldsymbol{\Phi}) \boldsymbol{\Phi}, \tag{1.2}$$

where $\boldsymbol{\Phi} = (\Phi_1(t), \ldots, \Phi_M(t))^{\mathrm{T}}$ is the desired solution vector, where $\Phi_j(t)$ is the approximate solution at spatial position x_j; $\Delta x := x_{j+1} - x_j$ for $j = 1, \ldots, M$ is the uniform grid spacing; $(\Delta^- \boldsymbol{f})(\boldsymbol{\Phi}) \in \mathbb{R}^{NM}$ denotes the vector of numerical flux vector differences associated with the discretization of $\partial_x \boldsymbol{f}(\Phi)$; and $\boldsymbol{\mathcal{B}}(\boldsymbol{\Phi}) \in \mathbb{R}^{(NM)\times(NM)}$ is a block tridiagonal matrix arising from the discretization of $\partial_x(\boldsymbol{B}(\Phi)\partial_x \Phi)$. The precise algebraic forms of $(\Delta^- \boldsymbol{f})(\boldsymbol{\Phi})$ and $\boldsymbol{\mathcal{B}}(\boldsymbol{\Phi})$ are provided in [10]. Here we emphasize that the matrix $\boldsymbol{\mathcal{B}}$ inherits its discontinuous dependence on $\boldsymbol{\Phi}$ from that of $\boldsymbol{B}$ on Φ.

The new approach is based on carefully distinguishing in (1.2) between stiff and nonstiff dependence on the solution vector $\boldsymbol{\Phi}$, and in choosing the time discretization by an implicit and an explicit RK scheme, respectively, of an IMEX pair of schemes accordingly. Roughly speaking, in the product $\boldsymbol{\mathcal{B}}(\boldsymbol{\Phi})\boldsymbol{\Phi}$ the occurrence of the solution $\boldsymbol{\Phi}$ within $\boldsymbol{\mathcal{B}}(\boldsymbol{\Phi})$ is considered nonstiff, while that of the factor $\boldsymbol{\Phi}$ is considered stiff. Thus, the implicit treatment is applied only to that second factor, in contrast to [10], where the whole expression $\boldsymbol{\mathcal{B}}(\boldsymbol{\Phi})\boldsymbol{\Phi}$ is treated implicitly. This new approach does not require solutions for *nonlinear* systems (in contrast to the approach of [10]), since the new methods require only solving a discretized convection-diffusion equation

with a *linear* diffusion term in which the matrix $\mathcal{B}$ is given. We therefore address the new methods introduced herein as *linearly implicit* IMEX-RK methods, in contrast to the methods of [10], to which we refer as *nonlinearly implicit* IMEX-RK methods. Numerical examples demonstrate that the new linearly implicit methods, which are much easier to implement, approximate the same solutions as the nonlinearly implicit ones, and in many cases are more efficient.

1.2. Related work. One could discretize the problem (1.1) in space only, obtaining a method of lines formulation that can be treated by some ODE solver. It is natural to treat the diffusion term implicitly, while maintaining the (possibly nonlinear) explicit treatment of the convection term. This has been realized by adopting IMEX-RK schemes [10]. References of the application of IMEX-RK schemes to hyperbolic systems with relaxation and the solution of semidiscretized partial differential equations include [6, 5, 7, 8, 25] and [1, 18, 21, 25, 27, 29], respectively. Results produced by IMEX-RK schemes are compared with those generated by the Kurganov–Tadmor (KT) high-resolution central difference scheme [22]. In the original approach of the KT method, both convection and diffusion are treated explicitly [22, sect. 4.2], and the time step is then restricted by stability rather than accuracy constraints.

First-order models of the type

$$\partial_t \Phi + \partial_x \boldsymbol{f}(\Phi) = \mathbf{0}, \quad \boldsymbol{f}(\Phi) = \big(\phi_1 v_1(\Phi), \ldots, \phi_N v_N(\Phi)\big)^{\mathrm{T}}, \tag{1.3}$$

where Φ is the vector of partial densities or volume fractions and $v_1, \ldots, v_N$ are given velocity functions, arise as models of polydisperse sedimentation, multiclass vehicular traffic, and the settling of dispersions (see [10] for references). For these models, the eigenvectors and eigenvalues of the Jacobian $\mathcal{J}_{\boldsymbol{f}}(\Phi) = (\partial f_i(\Phi)/\partial \phi_j)_{1 \le i,j \le N}$ are usually not available in closed form. However, for some of them, and under determined circumstances, the eigenvalues of $\mathcal{J}_{\boldsymbol{f}}(\Phi)$ are provably real and interlace with the velocities v_i. This information is the key ingredient for the construction of efficient characteristicwise (spectral) weighted essentially nonoscillatory (WENO) schemes for (1.3), denoted "WENO-SPEC" according to [9, 12], which are employed herein to discretize the convective part of (1.1).

For models of polydisperse sedimentation, the diffusive terms leading to the form (1.1) describe the formation of compressible sediments (see [3]). In that paper, the system (1.1) was solved by the KT method. On the other hand, the diffusively corrected version of the MCLWR traffic model is derived in [10].

1.3. Outline of the paper. The remainder of the paper is organized as follows. In section 2, which is at the core of the paper, both variants of semi-implicit IMEX-RK schemes are introduced. After recalling the spatial discretization of (1.1) and providing some preliminary notation common to both versions (sections 2.1 and 2.2), we summarize in section 2.3 the nonlinearly implicit IMEX-RK methods for solving the system (1.1) introduced in [10]. Section 2.4 is devoted to the new linearly implicit IMEX-RK methods. Then, in section 2.5, we propose five classical second-order IMEX-RK schemes adopted in the literature (cf., e.g., [4, 25]) from which we generate nonlinearly implicit and linearly implicit versions for numerical tests, and we outline in section 2.6 a linear stability analysis for these schemes. In section 3 we recall the models that motivate the degenerate convection-diffusion equation (1.1), namely, a model of polydisperse sedimentation of equal-density particles that form compressible sediments (Model 1) and a multiclass diffusively corrected kinematic traffic flow model (Model 2). The models are the same as those discussed in [10], so we refer the reader to that paper for further explanations and references.

Numerical examples are presented in section 4. We first state some preliminaries in section 4.1 and compare in Examples 1 to 4 (sections 4.2 and 4.3) the performance of the new linearly implicit IMEX-RK scheme with that of the nonlinearly implicit one of [10] for a test case of Model 1 with $N = 3$. The same model, but with a smooth initial datum, is used in Example 5 (section 4.4) to assess the numerical order of accuracy of the linearly implicit IMEX-RK scheme. In section 4.5 we present one test case for Model 2 (also with $N = 3$), for which the IMEX-RK scheme turns out to be more efficient than the nonlinearly implicit version. Finally, some concluding remarks are collected in section 5.

2. Numerical schemes.

2.1. Spatial discretization. Throughout the paper, interval $[0, \mathcal{L}]$ is divided into M cells of equal size Δx, and the grip points x_i, for $i = 1, \ldots, M$, are located at the center of each cell. The discretization $\frac{1}{\Delta x}(\Delta^- \boldsymbol{f})(\boldsymbol{\Phi})$ of the convective term $\partial_x \boldsymbol{f}(\Phi)$ is computed using the WENO-SPEC finite difference scheme [9]. The numerical fluxes are obtained by fifth-order WENO reconstructions of characteristic fluxes. For the diffusive term $\partial_x(\boldsymbol{B}(\Phi)\partial_x\Phi)$ we use the same discretization as in [10, sect. 3.1], which provides second-order approximation in space for this term. The precise form of $\boldsymbol{B}(\Phi)$ will be given in section 3. With the notation $\boldsymbol{\Phi} = (\boldsymbol{\Phi}_1^{\mathrm{T}}, \ldots \boldsymbol{\Phi}_M^{\mathrm{T}})^{\mathrm{T}} \in \mathbb{R}^{MN}$, where $\boldsymbol{\Phi}_i(t) \approx \Phi(x_i, t) \in \mathbb{R}^N$, we can define the $M \times M$ block tridiagonal matrix $\boldsymbol{\mathcal{B}} = \boldsymbol{\mathcal{B}}(\boldsymbol{\Phi})$, with blocks of size $N \times N$, by

$$\big(\boldsymbol{\mathcal{B}}(\boldsymbol{\Phi})\boldsymbol{\Phi}\big)_i(t) = \big(\boldsymbol{B}_{i-1/2}\boldsymbol{\Phi}_{i-1} - (\boldsymbol{B}_{i-1/2} + \boldsymbol{B}_{i+1/2})\boldsymbol{\Phi}_i + \boldsymbol{B}_{i+1/2}\boldsymbol{\Phi}_{i+1}\big)(t)$$

for $i = 1, \ldots, M$, where $\boldsymbol{B}_{i+1/2} := \frac{1}{2}(\boldsymbol{B}(\boldsymbol{\Phi}_i) + \boldsymbol{B}(\boldsymbol{\Phi}_{i+1}))$. The terms $\boldsymbol{B}_{i\pm1/2}\boldsymbol{\Phi}_{i\pm1}$ for $i = 1$ and $i = M$ are modified according to the boundary conditions.

2.2. Time integrator. The pair of Butcher arrays of IMEX-RK methods for the time integration of (1.2) is given by

$$\begin{array}{c|c} \tilde{\boldsymbol{c}} & \tilde{\boldsymbol{A}} \\ \hline & \tilde{\boldsymbol{b}}^{\mathrm{T}} \end{array} \qquad \begin{array}{c|c} \boldsymbol{c} & \boldsymbol{A} \\ \hline & \boldsymbol{b}^{\mathrm{T}} \end{array},$$

where the $s \times s$ lower triangular matrices $\tilde{\boldsymbol{A}} = (\tilde{a}_{ij})$ (with $\tilde{a}_{ij} = 0$ for all $j \geq i$) and $\boldsymbol{A} = (a_{ij})$ (with $a_{ij} = 0$ for all $j > i$) are the matrices of the explicit and implicit parts of the method, respectively, while $\tilde{\boldsymbol{b}} = (\tilde{b}_1, \ldots, \tilde{b}_s)^{\mathrm{T}}$, $\tilde{\boldsymbol{c}} = (\tilde{c}_1, \ldots, \tilde{c}_s)^{\mathrm{T}}$, $\boldsymbol{b} = (b_1, \ldots, b_s)^{\mathrm{T}}$, and $\boldsymbol{c} = (c_1, \ldots, c_s)^{\mathrm{T}}$ are s-dimensional vectors of real coefficients, with $\tilde{\boldsymbol{c}}$ and $\boldsymbol{c}$ given by the usual relations

$$\tilde{c}_i = \sum_{j=1}^{i-1} \tilde{a}_{ij}, \quad c_i = \sum_{j=1}^{i} a_{ij}, \quad i = 1, \ldots, s.$$

Now we rewrite the semidiscrete formulation (1.2) in the form

$$\frac{\mathrm{d}\boldsymbol{\Phi}}{\mathrm{d}t} = C(\boldsymbol{\Phi}) + D(\boldsymbol{\Phi}), \tag{2.1}$$

where we define

$$C(\boldsymbol{\Phi}) := -\frac{1}{\Delta x}(\Delta^- \boldsymbol{f})(\boldsymbol{\Phi}), \quad D(\boldsymbol{\Phi}) := \frac{1}{\Delta x^2}\boldsymbol{\mathcal{B}}(\boldsymbol{\Phi})\boldsymbol{\Phi}. \tag{2.2}$$

An IMEX-RK scheme applied to (2.1) reads as

$$\begin{aligned}\boldsymbol{\Phi}^{(i)} &= \boldsymbol{\Phi}^n + \Delta t \sum_{j=1}^{i-1} \tilde{a}_{ij} C(\boldsymbol{\Phi}^{(j)}) + \Delta t \sum_{j=1}^{i} a_{ij} D(\boldsymbol{\Phi}^{(j)}),\\ \boldsymbol{\Phi}^{n+1} &= \boldsymbol{\Phi}^n + \Delta t \sum_{j=1}^{s} \tilde{b}_i C(\boldsymbol{\Phi}^{(i)}) + \Delta t \sum_{j=1}^{s} b_i D(\boldsymbol{\Phi}^{(i)}).\end{aligned} \tag{2.3}$$

We observe that in IMEX-RK schemes there is only one family of stage values. Furthermore, the fact that the implicit part of the method is a *diagonally implicit* RK (DIRK) scheme makes the implementation of an IMEX-RK scheme simpler and ensures that C is effectively computed explicitly.

Notice that the system (2.1) can be treated by another family of methods, called additive RK (ARK) schemes, introduced by Zhong (for details see [29]), and which have the following form:

$$K_i = C\left(\boldsymbol{\Phi}^n + \Delta t \sum_{j=1}^{i-1} \tilde{a}_{ij} K_j\right) + D\left(\boldsymbol{\Phi}^n + \Delta t \sum_{j=1}^{i-1} a_{ij} K_j + \Delta t a_{ii} K_i\right), \quad i = 1, \ldots, s, \tag{2.4}$$

$$\boldsymbol{\Phi}^{n+1} = \boldsymbol{\Phi}^n + \Delta t \sum_{i=1}^{s} b_i K_i. \tag{2.5}$$

It is easy to show that ARK schemes can been seen as a particular case of IMEX-RK schemes, obtained by introducing two families of stage values, respectively, for the explicit and implicit parts (see [4]). ARK schemes allow a linearly implicit form which is particularly efficient, since the implicit term is linear and entails no loss of order of accuracy or stability. A further generalization of the above approaches is given by the *generalized additively* partitioned RK (GARK) schemes [15].

Next we present and describe two different approaches for solving (1.1), i.e., the nonlinearly implicit IMEX-RK methods and the linearly implicit IMEX-RK ones, where the first is based on the IMEX-RK framework (2.3), while the second is a semi-implicit variant of the ARK approach (2.4), (2.5).

2.3. Nonlinearly implicit IMEX-RK methods. To summarize the nonlinearly implicit IMEX-RK (NI-IMEX-RK) method for solving (1.1) introduced in [10], we consider the semidiscrete formulation (2.1), (2.2).

The simplest IMEX scheme for the approximation of (1.2) is

$$\boldsymbol{\Phi}^{n+1} = \boldsymbol{\Phi}^n - \frac{\Delta t}{\Delta x}(\Delta^- \boldsymbol{f})(\boldsymbol{\Phi}^n) + \frac{\Delta t}{\Delta x^2} \boldsymbol{\mathcal{B}}(\boldsymbol{\Phi}^{n+1}) \boldsymbol{\Phi}^{n+1}, \tag{2.6}$$

where $\boldsymbol{\Phi}^n$ denotes the approximate value of $\boldsymbol{\Phi}(t)$ at $t = t^n$. In general, the computations of an NI-IMEX-RK scheme necessary to advance $\boldsymbol{\Phi}^n$ from time t^n to $t^{n+1} = t^n + \Delta t$ in system (2.1)–(2.2) are given in Algorithm 2.1 [1, 25] (cf. [10]).

ALGORITHM 2.1 (NI-IMEX-RK scheme [10]).

Input: approximate solution vector $\boldsymbol{\Phi}^n$ *for* $t = t_n$

do $i = 1, \ldots, s$

solve for $\boldsymbol{\Phi}^{(i)}$ *the nonlinear equation*

$$\boldsymbol{\Phi}^{(i)} = \boldsymbol{\Phi}^n + \Delta t \left(\sum_{j=1}^{i-1} a_{ij} K_j + a_{ii} D\big(\boldsymbol{\Phi}^{(i)}\big) + \sum_{j=1}^{i-1} \tilde{a}_{ij} \tilde{K}_j \right)$$

$K_i \leftarrow D(\mathbf{\Phi}^{(i)})$
$\tilde{K}_i \leftarrow C(\mathbf{\Phi}^{(i)})$
enddo
$\mathbf{\Phi}^{n+1} \leftarrow \mathbf{\Phi}^n + \Delta t \sum_{j=1}^{s} b_j K_j + \Delta t \sum_{j=1}^{s} \tilde{b}_j \tilde{K}_j$
Output: approximate solution vector $\mathbf{\Phi}^{n+1}$ *for* $t = t^{n+1} = t^n + \Delta t$.

Algorithm 2.1 requires solving for the vector $\boldsymbol{u} = \mathbf{\Phi}^{(i)} \in \mathbb{R}^{MN}$, a nonlinear system of NM scalar equations of the following form:

$$\mathbf{\Psi}_i(\boldsymbol{u}) := \boldsymbol{u} - a_{ii}\Delta t D\big(\boldsymbol{u}\big) - \boldsymbol{r}_i = \mathbf{0}, \quad i = 1, \ldots, s, \tag{2.7}$$

where $\boldsymbol{r}_i \in \mathbb{R}^{MN}$ is given by

$$\boldsymbol{r}_i = \mathbf{\Phi}^n + \Delta t \left(\sum_{j=1}^{i-1} a_{ij} K_j + \sum_{j=1}^{i-1} \tilde{a}_{ij} \tilde{K}_j \right).$$

For simplicity, we shall drop the index i in $\mathbf{\Psi}_i$ for $i = 1, \ldots, s$ for the rest of the discussion. To approximately solve (2.7) by the NR iterative method we must require the coefficients of $\boldsymbol{B}$, and therefore those of $\boldsymbol{\mathcal{B}}$, to be at least continuously differentiable [24, p. 311]. However, the models of interest herein (to be introduced in section 3) do not naturally satisfy this assumption. Therefore $\boldsymbol{B}$ is replaced by a smooth approximation $\boldsymbol{B}_\varepsilon$, and we denote the corresponding version of $\boldsymbol{\mathcal{B}}$ by $\boldsymbol{\mathcal{B}}_\varepsilon$, where $\boldsymbol{B}_\varepsilon \to \boldsymbol{B}$ and $\boldsymbol{\mathcal{B}}_\varepsilon \to \boldsymbol{\mathcal{B}}$ as $\varepsilon \to 0$. We propose in [10] the following strategy to efficiently solve $\mathbf{\Psi}_\varepsilon(\boldsymbol{u}) = \mathbf{0}$ for a prescribed $\varepsilon = \varepsilon_{\min}$: if $\boldsymbol{u}_\varepsilon$ is a solution of $\mathbf{\Psi}_\varepsilon(\boldsymbol{u}_\varepsilon) = \mathbf{0}$, then $\boldsymbol{u}_\varepsilon$ is used as an initial datum for approximating the solution of $\mathbf{\Psi}_{\varepsilon'}(\boldsymbol{u}) = \mathbf{0}$ for $\varepsilon' < \varepsilon$ by the NR method with a line search strategy [11]. This process is started with a sufficiently large value ε_0 and is performed until a solution $\mathbf{\Psi}_{\varepsilon_{\min}}(\boldsymbol{u}) = \mathbf{0}$ is obtained. See Algorithm 4.1 of [10] for details.

2.4. Linearly implicit IMEX-RK methods. The NI-IMEX-RK schemes proposed in [10], and whose simplest variant is (2.6), require solving a nonlinear system of NM scalar equations (cf. Algorithm 2.1). To overcome this excessive numerical work for the solution of the nonlinear system (2.7), an essential gain is obtained by the following approach. We rewrite the semidiscrete formulation (1.2) in the form

$$\frac{\mathrm{d}\mathbf{\Phi}}{\mathrm{d}t} = \mathcal{K}(\mathbf{\Phi}^*, \mathbf{\Phi}), \tag{2.8}$$

with

$$\mathcal{K}(\mathbf{\Phi}^*, \mathbf{\Phi}) = C(\mathbf{\Phi}^*) + \frac{1}{\Delta x^2} \boldsymbol{\mathcal{B}}(\mathbf{\Phi}^*)\mathbf{\Phi},$$

with C given in (2.2), and we observe that the only stiff term is the linear term $\mathbf{\Phi}$ that multiplies $\mathcal{B}(\mathbf{\Phi}^*)$. We therefore treat $\mathbf{\Phi}^*$ explicitly as an argument of $\boldsymbol{f}$ and $\boldsymbol{\mathcal{B}}$, while $\mathbf{\Phi}$ is implicit in the term to which $\boldsymbol{\mathcal{B}}$ is applied.

The schemes (2.4) can be extended to the more general equation (2.8). Consider an autonomous equation of the form

$$\frac{\mathrm{d}\boldsymbol{y}}{\mathrm{d}t} = \mathcal{K}(\boldsymbol{y}^*, \boldsymbol{y}), \tag{2.9}$$

where the function $\mathcal{K} : \mathbb{R}^m \times \mathbb{R}^m \to \mathbb{R}^m$ is supposed to be sufficiently differentiable. Suppose that the dependence on the first argument of $\mathcal{K}$ is nonstiff, while that on the second argument is stiff. Such a system can be rewritten in the form

$$\frac{\mathrm{d}\boldsymbol{y}^*}{\mathrm{d}t} = \mathcal{K}(\boldsymbol{y}^*, \boldsymbol{y}), \quad \frac{\mathrm{d}\boldsymbol{y}}{\mathrm{d}t} = \mathcal{K}(\boldsymbol{y}^*, \boldsymbol{y}), \tag{2.10}$$

with $\boldsymbol{y}^*(t_0) = \boldsymbol{y}(t_0) = \boldsymbol{y}_0$. This system is a particular case of *partitioned system* [16], but with an additional computational cost since we double the number of variables.

Now let us apply an IMEX scheme to (2.10). This results in the formulas

$$\boldsymbol{Y}_i^* = \boldsymbol{y}_n^* + \Delta t \sum_{j=1}^{i-1} \tilde{a}_{ij} \mathcal{K}(\boldsymbol{Y}_j^*, \boldsymbol{Y}_j), \quad \boldsymbol{Y}_i = \boldsymbol{y}_n + \Delta t \sum_{j=1}^{i} a_{ij} \mathcal{K}(\boldsymbol{Y}_j^*, \boldsymbol{Y}_j),$$
$$\boldsymbol{y}_{n+1}^* = \boldsymbol{y}_n^* + \Delta t \sum_{i=1}^{s} \tilde{b}_i \mathcal{K}(\boldsymbol{Y}_i^*, \boldsymbol{Y}_i), \quad \boldsymbol{y}_{n+1} = \boldsymbol{y}_n + \Delta t \sum_{i=1}^{s} b_i \mathcal{K}(\boldsymbol{Y}_i^*, \boldsymbol{Y}_i).$$

Observe that if $\tilde{\boldsymbol{b}} = \boldsymbol{b}$, then $\boldsymbol{y}_n^* = \boldsymbol{y}_n$ for all $n \geq 0$, and therefore the duplication of variables is not necessary if we adopt the RK fluxes $K_i = \mathcal{K}(\boldsymbol{Y}_i^*, \boldsymbol{Y}_i)$ as basic unknowns, so that one can rewrite the scheme in the form

$$K_i = \mathcal{K}\left(\boldsymbol{y}_n + \Delta t \sum_{j=1}^{i-1} \tilde{a}_{ij} K_j, \boldsymbol{y}_n + \Delta t \sum_{j=1}^{i-1} a_{ij} K_j + \Delta t a_{ii} K_i\right), \quad i = 1, \ldots, s, \tag{2.11}$$

with the numerical solution

$$\boldsymbol{y}_{n+1} = \boldsymbol{y}_n + \Delta t \sum_{i=1}^{s} b_i K_i. \tag{2.12}$$

Notice that with the choice $\mathcal{K}(\Phi^*, \Phi) = C(\Phi^*) + D(\Phi)$, the approach reduces to the one proposed by Zhong [29], requiring the solution of nonlinear systems.

Because of the formal equivalence with partitioned systems, order conditions for ARK schemes can be derived from those for IMEX-RK schemes. High order in time can be obtained by adopting IMEX-RK schemes with $\tilde{\boldsymbol{b}} = \boldsymbol{b}$. For a more general description of the relation between IMEX and ARK methods, see [4].

In light of the previous discussion, the simplest first-order LI-IMEX-RK scheme for (2.11), (2.12) is

$$\boldsymbol{\Phi}^{n+1} = \boldsymbol{\Phi}^n - \frac{\Delta t}{\Delta x}(\Delta^- \boldsymbol{f})(\boldsymbol{\Phi}^n) + \frac{\Delta t}{\Delta x^2} \boldsymbol{\mathcal{B}}(\boldsymbol{\Phi}^n) \boldsymbol{\Phi}^{n+1}.$$

Now by (2.11) and (2.12) the step from t^n to $t^{n+1} = t^n + \Delta t$ of the new linearly implicit IMEX-RK (LI-IMEX-RK) scheme is given by the following algorithm.

ALGORITHM 2.2 (LI-IMEX-RK scheme).

Input: approximate solution vector $\boldsymbol{\Phi}^n$ *for* $t = t^n$

do $i = 1, \ldots, s$

compute the stage values:

$$\boldsymbol{\Phi}^{*(i)} \leftarrow \boldsymbol{\Phi}^n + \Delta t \sum_{j=1}^{i-1} \tilde{a}_{ij} K_j$$

$$\hat{\boldsymbol{\Phi}}^{(i)} \leftarrow \boldsymbol{\Phi}^n + \Delta t \sum_{j=1}^{i-1} a_{ij} K_j$$

solve for K_i the linear system

$$K_i = C\big(\mathbf{\Phi}^{*(i)}\big) + \frac{1}{\Delta x^2}\boldsymbol{\mathcal{B}}\big(\mathbf{\Phi}^{*(i)}\big)\Big(\hat{\mathbf{\Phi}}^{(i)} + \Delta t a_{ii} K_i\Big) \tag{2.13}$$

enddo

$$\mathbf{\Phi}^{n+1} \leftarrow \mathbf{\Phi}^n + \Delta t \sum_{j=1}^{s} b_j K_j$$

Output: approximate solution vector $\mathbf{\Phi}^{n+1}$ for $t = t^{n+1} = t^n + \Delta t$.

The decisive advantage of the new linearly implicit approach for computing the numerical solution of system (2.8) is obvious: we do not require solutions for any nonlinear system, such as, for example, (2.7) (corresponding to (3.7) in [10]). In this new approach, the system (2.13) is linear in K_i and the numerical solution can be obtained by solving a convection-diffusion equation with a linear diffusion term in which the matrix function $\boldsymbol{B}$, and therefore $\boldsymbol{\mathcal{B}}$, is computed explicitly.

2.5. Some second-order IMEX-RK schemes. In our numerical tests we use the following five second-order schemes. The first one is the combination of the Heun method and the trapezoidal rule, called H-CN(2,2,2); see Table 1(a). The second scheme is the combination of the Heun method and an A-stable second-order DIRK method, called H-DIRK2(2,2,2); see Table 1(b). The next two schemes are based on the Heun method coupled with L-stable DIRK methods, introduced in [25], namely, the schemes H-LDIRKp(2,2,2) for $p = 2$ and $p = 3$; see Table 1(c). The version for $p = 2$ also has the strongly stability preserving (SSP) property. The choice of γ for $p = 3$ guarantees that the implicit part is a third-order DIRK scheme with the best dampening properties [16]. The last scheme is obtained by combining a three-stage, second-order SSP scheme with an L-stable, second-order DIRK scheme and is denoted by SSP-LDIRK(3,3,2); see Table 1(d). As we shall see, this scheme has a wider stability region, at the price of one extra level.

Notice that the scheme H-CN(2,2,2) is a natural choice when dealing with a convection-diffusion equation, since the Heun method is an SSP explicit RK one [14], and the trapezoidal rule (also known as Crank–Nicolson) is A-stable and widely used for diffusion problems. The two schemes H-LDIRK2(2,2,2) and SSP-LDIRK(3,3,2) were introduced in the context of hyperbolic systems with stiff relaxation [25].

TABLE 1
The second-order IMEX-RK schemes we adopt in this paper [4, 25].

(a) Scheme H-CN(2,2,2)

0	0	0
1	1	0
	$\frac{1}{2}$	$\frac{1}{2}$

0	0	0
1	$\frac{1}{2}$	$\frac{1}{2}$
	$\frac{1}{2}$	$\frac{1}{2}$

(b) Scheme H-DIRK2(2,2,2)

0	0	0
1	1	0
	$\frac{1}{2}$	$\frac{1}{2}$

$\frac{1}{2}$	$\frac{1}{2}$	0
$\frac{1}{2}$	0	$\frac{1}{2}$
	$\frac{1}{2}$	$\frac{1}{2}$

(c) Schemes H-LDIRKp(2,2,2)

0	0	0
1	1	0
	$\frac{1}{2}$	$\frac{1}{2}$

γ	γ	0
$1-\gamma$	$1-2\gamma$	γ
	$\frac{1}{2}$	$\frac{1}{2}$

$$\gamma = \begin{cases} 1 - 1/\sqrt{2} & \text{for } p = 2, \\ (3+\sqrt{3})/6 & \text{for } p = 3 \end{cases}$$

(d) Scheme SSP-LDIRK(3,3,2)

0	0	0	0
$\frac{1}{2}$	$\frac{1}{2}$	0	0
1	$\frac{1}{2}$	$\frac{1}{2}$	0
	$\frac{1}{3}$	$\frac{1}{3}$	$\frac{1}{3}$

$\frac{1}{4}$	$\frac{1}{4}$	0	0
$\frac{1}{4}$	0	$\frac{1}{4}$	0
1	$\frac{1}{3}$	$\frac{1}{3}$	$\frac{1}{3}$
	$\frac{1}{3}$	$\frac{1}{3}$	$\frac{1}{3}$

2.6. Linear stability analysis. There is no general notion of stability for IMEX schemes, even if one restricts the discussion to the linear case [1, 13, 17, 21, 23, 26, 29]. Here we limit ourselves to a linear stability analysis for the complex scalar equation, which is usually adopted in the classical definitions of A-stability for RK schemes [16]. We show that IMEX-RK and ARK have the same stability function and analyze the stability region for all schemes that we use in the paper. We are aware of the limitation of this analysis with respect to the case of classical RK methods. For example, stability results for the scalar equation cannot be exported to linear systems of the form $\boldsymbol{y}' = \mathbf{A}\boldsymbol{y} + \mathbf{B}\boldsymbol{y}$, with $\mathbf{A}$ and $\mathbf{B}$ being real square matrices, unless the two matrices share a basis of eigenvectors. In spite of such limitations, we believe that linear stability gives some information useful in comparing the various schemes.

LEMMA 2.1. *If the IMEX scheme defined by* (2.11), (2.12) *is applied to the autonomous equation* (2.9) *in the scalar case* ($m = 1$) *with*

$$\mathcal{K}(y^*, y) = \lambda y^* + \mu y, \quad \lambda, \mu \in \mathbb{C}, \tag{2.14}$$

then the iterates y_n *satisfy* $y_{n+1} = R(z_1, z)y_n$, *where* $z_1 = \lambda\Delta t$, $z = \mu\Delta t$, *and*

$$R(z_1, z) = 1 + (z_1 + z)\boldsymbol{b}^{\mathrm{T}}(\boldsymbol{I} - z_1\tilde{\boldsymbol{A}} - z\boldsymbol{A})^{-1}\boldsymbol{e}. \tag{2.15}$$

Here $\boldsymbol{I}$ *denotes the* $s \times s$ *identity matrix and* $\boldsymbol{e} = (1, \dots, 1)^{\mathrm{T}} \in \mathbb{R}^s$.

Proof. Expression (2.11) for (2.9), (2.14), and $m = 1$ reads as

$$K_i = \lambda\left(y_n + \Delta t \sum_{i<j} \tilde{a}_{ij} K_j\right) + \mu\left(y_n + \Delta t \sum_{i\le j} a_{ij} K_j\right), \quad i = 1, \dots, s.$$

For $K := (K_1, \dots, K_s)^{\mathrm{T}}$ we get $K = (\lambda + \mu)y_n(\boldsymbol{I} - z_1\tilde{\boldsymbol{A}} - z\boldsymbol{A})^{-1}\boldsymbol{e}$. Inserting this into (2.12) yields

$$y_{n+1} = y_n + \Delta t\boldsymbol{b}^{\mathrm{T}}K = \big(1 + (z_1 + z)\boldsymbol{b}^{\mathrm{T}}(\boldsymbol{I} - z_1\tilde{\boldsymbol{A}} - z\boldsymbol{A})^{-1}\boldsymbol{e}\big)y_n. \qquad \square$$

The A-stability region of the semi-implicit RK scheme (2.11) and (2.12) in the complex plane is defined as

$$S_A = \big\{(z_1, z) \in \mathbb{C}^2 : \big|R(z_1, z)\big| \le 1\big\}.$$

In this paper we adopt the definition of stability region given in [23], namely,

$$S_1 = \big\{z_1 \in \mathbb{C} : \sup_{z\in\mathbb{C}^-}\big|R(z_1, z)\big| \le 1\big\}, \tag{2.16}$$

which has the following motivations: we look for a simpler stability region which is a subset of $\mathbb{C}$ rather than $\mathbb{C}^2$. Since the implicit part of the method is A-stable, it is reasonable to look for the region $z_1 \in \mathbb{C}$ such that the scheme remains A-stable, i.e., $|R(z_1, z)| \le 1$ for all $z \in \mathbb{C}$.

Notice that when $z = 0$ we obtain the classical stability function of an explicit RK method, i.e.,

$$R(z_1, 0) = 1 + z_1\sum_{i=1} b_i + z_1^2\sum_{i,j} b_i\tilde{a}_{ij} + z_1^3\sum_{i,j,k} b_i\tilde{a}_{ij}\tilde{a}_{jk} + \cdots.$$

Some of the schemes adopted in this paper are L-stable in the implicit part, which means that $R(z_1, z) = 0$ as $z \to \infty$, and this implies that the coefficients of the

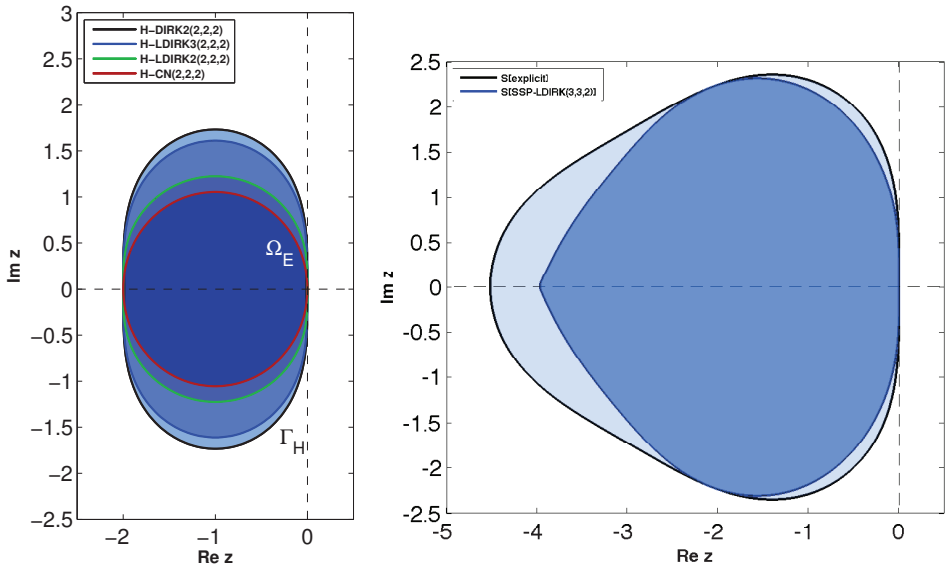

FIG. 1. *Stability regions S_1 of the IMEX schemes adopted in the paper. Left panel:* (2,2,2) *schemes H-DIRK*2*, H-LDIRK*3*, H-LDIRK*2*, and H-CN. Right panel: Scheme SSP-LDIRK*(3,3,2)*, and the corresponding explicit RK method when* $z = 0$*. (See electronic version for color.)*

semi-implicit scheme (2.11) and (2.12) satisfy the following condition (see [29] for details):

$$1 + \sum_{i=1}^{s} b_i \beta_i = 0, \quad \text{where} \quad \beta_i = -\frac{1}{a_{ii}} \left(1 + \sum_{j=1}^{i-1} a_{ij} \beta_j \right), \quad i = 1, \ldots, s. \tag{2.17}$$

Note that the coefficients of the schemes H-LDIRKp(2,2,2) and SSP-LDIRK(3,3,2) satisfy (2.17), while those of schemes H-CN(2,2,2) and H-DIRK2(2,2,2) do not.

In the left panel of Figure 1 we plot the stability regions of the four two-stage schemes adopted in the paper. We observe that the stability region of H-DIRK2(2,2,2) coincides exactly with the classical stability region of a second-order, two-level explicit RK method, whose stability function is $R(z_1) = 1 + z_1 + z_1^2/2$, and the stability region of H-CN(2,2,2) coincides with that of the explicit Euler method. We prove these facts in Theorems B.1 and B.2 in Appendix B. The right panel of Figure 1 displays the stability region S_1 of scheme SSP-LDIRK(3,3,2) (the boundary is marked by a blue line; see electronic version for color) and the corresponding region of the explicit RK method, whose stability function is $R(z_1) = 1 + z_1 + z_1^2/2 + z_1^3/12$ (black line), i.e., $R(z_1, 0)$.

3. Multispecies kinematic flow models. Model 1 describes the sedimentation of a polydisperse suspension of equal-density particles belonging to N species with sizes $d_1 > d_2 > \cdots > d_N$. We let ϕ_i denote the local volume fraction of species i having size d_i. The evolution of $\Phi = \Phi(x, t)$ as a function of depth x and time t in a column of height $\mathcal{L}$ is then determined by (1.1) posed on the x-interval $(0, \mathcal{L})$ for $t > 0$, along with $\Phi(x, 0) = \Phi_0(x)$ for $0 \le x \le \mathcal{L}$, where Φ_0 is the given initial

concentration distribution, and zero-flux boundary conditions, i.e.,

$$\boldsymbol{f}(\Phi) - \boldsymbol{B}(\Phi)\partial_x \Phi = \mathbf{0} \quad \text{for } x = 0 \text{ and } x = \mathcal{L}, \quad t > 0. \tag{3.1}$$

The flux density functions $f_1, \ldots, f_N$ are given by

$$f_i(\Phi) = \mu \bar{\varrho}_{\mathrm{s}} \phi_i V(\phi)(1-\phi)(\delta_i - \boldsymbol{\delta}^{\mathrm{T}}\Phi), \quad i = 1, \ldots, N, \tag{3.2}$$

where $\mu > 0$ is a viscosity constant, $\bar{\varrho}_{\mathrm{s}} > 0$ is the solid mass density minus the fluid density, $\delta_i := d_i^2/d_1^2$, $\boldsymbol{\delta} := (\delta_1, \delta_2, \ldots, \delta_N)^{\mathrm{T}}$, $\delta_1 = 1$, $\phi := \phi_1 + \cdots + \phi_N$, and $V(\phi)$ is a hindered settling function that can be chosen as

$$V(\phi) = \begin{cases} (1-\phi)^{n_{\mathrm{RZ}}-2} & \text{for } 0 \le \phi \le \phi_{\max}, \\ 0 & \text{otherwise,} \end{cases}$$

where $n_{\mathrm{RZ}} > 2$ is a material-dependent exponent.

The diffusion matrix is given by $\boldsymbol{B}(\Phi) := (\alpha_{ij})_{1 \le i,j \le N}$, where

$$\begin{aligned} \alpha_{ij} = \frac{\mu V(\phi)}{g\phi} \Big\{ & (1-\phi)\phi_i(\delta_i - \boldsymbol{\delta}^{\mathrm{T}}\Phi)\sigma_{\mathrm{e}}'(\phi) \\ & - \left[\delta_i \delta_{ij} - \delta_j \phi_i - \frac{\phi_i}{\phi}(\delta_i - \boldsymbol{\delta}^{\mathrm{T}}\Phi) \right] \sigma_{\mathrm{e}}(\phi) \Big\}, \quad i,j = 1, \ldots, N, \end{aligned} \tag{3.3}$$

where δ_{ij} is the standard Kronecker symbol and σ_{e} denotes the effective solid stress function, and σ_{e}' is its derivative. This function can be chosen as

$$\sigma_{\mathrm{e}}(\phi) = \begin{cases} 0 & \text{for } \phi \le \phi_{\mathrm{c}}, \\ \sigma_0\big((\phi/\phi_{\mathrm{c}})^k - 1\big) & \text{for } \phi > \phi_{\mathrm{c}}, \end{cases} \quad \sigma_0, k > 0, \tag{3.4}$$

where ϕ_{c} is a critical concentration at which the particles touch each other. Clearly, (3.3) and (3.4) imply that $\boldsymbol{B}(\Phi) = \mathbf{0}$ whenever $\phi \le \phi_{\mathrm{c}}$, so (1.1) is usually strongly degenerate under the assumptions of Model 1. Otherwise the eigenvalues of $\boldsymbol{B}(\Phi)$ are positive and pairwise distinct [3, Thm. 4.3].

For Model 2, a diffusively corrected MCLWR model, we assume that $v_i^{\max}$ is the preferred velocity of vehicle class i, where $v_1^{\max} > v_2^{\max} > \cdots > v_N^{\max} > 0$. If ϕ_i is the local density of class i, then the local velocity v_i of vehicles of class i is given by $v_i = v_i^{\max} V(\phi)$, where $\phi = \phi_1 + \cdots + \phi_N$ and V is a nonincreasing function that describes a driver's attitude to reduce velocity in the presence of other cars. Thus, the standard MCLWR model (without diffusive correction) is given by (1.3), where

$$f_i(\Phi) = \phi_i v_i^{\max} V(\phi), \quad i = 1, \ldots, N, \tag{3.5}$$

along with periodic boundary conditions as for a circular road of length $\mathcal{L}$, i.e.,

$$\Phi(0,t) = \Phi(\mathcal{L}, t), \quad t > 0. \tag{3.6}$$

The assumption that drivers exhibit an anticipation distance L and a reaction time τ leads to a system of the form (1.1), where $\boldsymbol{f}(\Phi)$ is given by (3.5) and the diffusion matrix $\boldsymbol{B}(\Phi)$ is now given by $\boldsymbol{B}(\Phi) := (\alpha_{ij})_{1 \le i,j \le N}$ with

$$\alpha_{ij}(\Phi) = -V'(\phi)\big[L + \tau\big(V'(\phi)(\boldsymbol{v}^{\max})^{\mathrm{T}}\Phi + \big(v_j^{\max} - v_i^{\max}\big)V(\phi)\big)\big]\phi_i v_i^{\max}. \tag{3.7}$$

The MCLWR model (1.1) is strictly hyperbolic for $\boldsymbol{B} \equiv 0$ and is hyperbolic-parabolic if some conditions on τ and L hold (see [10] for the specific details).

A common choice of $V = V(\phi)$ in traffic modeling is the model

$$V(\phi) = V_{\mathrm{DG}}(\phi) = \begin{cases} 1, & \phi \le \phi_{\mathrm{c}}, \\ \ln \phi / \ln \phi_{\mathrm{c}}, & \phi > \phi_{\mathrm{c}}. \end{cases} \tag{3.8}$$

Since $V'(\phi) = 0$ for $0 \le \phi \le \phi_{\mathrm{c}}$, using model (3.8) in (3.7) means that $\boldsymbol{B}(\Phi) = \boldsymbol{0}$ for $\phi \le \phi_{\mathrm{c}}$ also holds for Model 2, i.e., (1.1) again becomes strongly degenerate.

We remark that for both Model 1 with $\sigma_{\mathrm{e}}(\phi)$ defined by (3.4) and Model 2 with $V(\phi)$ defined by (3.8), the diffusion matrix $\boldsymbol{B}(\Phi)$ is discontinuous at $\phi = \phi_{\mathrm{c}}$. This property is explicitly included in the well-posedness analysis available for (1.1) in the *scalar* case (cf., e.g., [19, 20]).

4. Numerical results.

4.1. Preliminaries. In the following examples, we solve (1.1) numerically for $0 \le t \le T$ and $0 \le x \le \mathcal{L}$ for Models 1 and 2. We compare numerical results obtained by the NI-IMEX-RK schemes, denoted here "NI-H-CN(2,2,2)," "NI-H-DIRK2(2,2,2)," and so on according to the respective underlying IMEX-RK scheme (see Table 1), where we also omit the insertion "IMEX" for brevity, with those obtained by the new LI-IMEX-RK schemes of section 2.4, denoted correspondingly by "LI-H-CN(2,2,2)," "LI-H-DIRK2(2,2,2)," etc. Moreover results are compared with those generated by the explicit KT method [22].

For each model, the x-interval $[0, \mathcal{L}]$ is subdivided into M subintervals of length $\Delta x = \mathcal{L}/M$. We denote by Δt the time step used to advance the numerical solution from $t = t^n$ to $t^{n+1} = t^n + \Delta t$ and by Φ_j^n the vector of numerical solutions associated with cell $[j\Delta x, (j+1)\Delta x]$, $j = 0, \ldots, M-1$, at time t^n. For each iteration, Δt is determined by the following formula (derived from a linearized CFL condition):

$$\frac{\Delta t}{\Delta x} \max_{1 \le j \le M} \varrho\big(\mathcal{J}_{\boldsymbol{f}}(\Phi_j^n)\big) + \frac{\Delta t}{2\Delta x^2} \max_{1 \le j \le M} \varrho\big(\boldsymbol{B}(\Phi_j^n)\big) = C_{\mathrm{cfl}_1}$$

for the KT scheme and

$$\frac{\Delta t}{\Delta x} \max_{1 \le j \le M} \varrho\big(\mathcal{J}_{\boldsymbol{f}}(\Phi_j^n)\big) = C_{\mathrm{cfl}_2}$$

for the semi-implicit schemes, where $\varrho(\cdot)$ is the spectral radius. In the numerical examples we choose C_{cfl_*} as the largest multiple of 0.05 that yields oscillation-free numerical solutions.

For comparison purposes, we compute reference solutions for numerical tests by the KT scheme with $M_{\mathrm{ref}} = 25600$ cells. As in [10], we compute approximate L^1 errors at different times for each scheme as follows. We denote by $(\phi_{j,i}^M(t))_{j=1}^M$ and $(\phi_{l,i}^{\mathrm{ref}}(t))_{l=1}^{M_{\mathrm{ref}}}$ the numerical solution for the ith component at time t calculated with M and M_{ref} cells, respectively. We use cubic interpolation from the reference grid to the M-cell grid to compute $\tilde{\phi}_{j,i}^{\mathrm{ref}}(t)$ for $j = 1, \ldots, M$. The total approximate L^1 error of the numerical solution on the M-cell grid at time t is then given by

$$e_M^{\mathrm{tot}}(t) := \frac{1}{M} \sum_{i=1}^{N} \sum_{j=1}^{M} \big| \tilde{\phi}_{j,i}^{\mathrm{ref}}(t) - \phi_{j,i}^M(t) \big|. \tag{4.1}$$

Based on the errors defined by (4.1), we may calculate a numerical order of convergence from pairs of total approximate L^1 errors $e_M^{\mathrm{tot}}(t)$ and $e_{2M}^{\mathrm{tot}}(t)$ by

$$\theta_M(t) := \log_2\big(e_M^{\mathrm{tot}}(t)/e_{2M}^{\mathrm{tot}}(t)\big). \tag{4.2}$$

To demonstrate that our way of calculating approximate errors and estimating convergence rates leads to conclusions that are independent of the particular reference solution, we employ in one case (Example 5) an alternative way of calculating approximate errors and convergence rates; namely, we use cubic interpolation from the grid of $2M$ cells that of M cells grid to compute the quantities

$$\tilde{\phi}_{j,i}^M(t) = \frac{9}{16}\big(\phi_{2j,i}^{2M} + \phi_{2j-1,i}^{2M}\big) - \frac{1}{16}\big(\phi_{2j+1,i}^{2M} + \phi_{2j-2,i}^{2M}\big), \quad j = 1, \dots, M, \tag{4.3}$$

because $x_j^M = (x_{2j}^{2M} + x_{2j-1}^{2M})/2$.

We then calculate an alternative (to (4.1)) total approximate L^1 error by

$$\hat{e}_M^{\mathrm{tot}}(t) := \frac{1}{M}\sum_{i=1}^{N}\sum_{j=1}^{M}\big|\tilde{\phi}_{j,i}^M(t) - \phi_{j,i}^M(t)\big|. \tag{4.4}$$

An alternative numerical order of convergence can then be computed by

$$\hat{\theta}_M(t) := \log_2\big(\hat{e}_M^{\mathrm{tot}}(t)/\hat{e}_{2M}^{\mathrm{tot}}(t)\big). \tag{4.5}$$

(Note carefully that $\hat{\theta}_M(t)$ is calculated from the three numerical solutions calculated on grids with M, $2M$, and $4M$ cells.) Since the scheme is second-order accurate for smooth solutions, an estimate of the (unknown) total exact L^1 error

$$e_M^{\mathrm{tot},*}(t) := \frac{1}{M}\sum_{i=1}^{N}\sum_{j=1}^{M}\big|\phi_i(x_j,t) - \phi_{j,i}^M(t)\big| \tag{4.6}$$

is given by

$$e_M^{\mathrm{tot},*}(t) \approx \tilde{e}_M^{\mathrm{tot}}(t) := \frac{4}{3}\hat{e}_M^{\mathrm{tot}}(t). \tag{4.7}$$

The motivation of (4.3)–(4.7) is briefly recalled in the appendix.

4.2. Example 1: Model 1 with $N = 3$, comparison of LI- and NI-IMEX-SSP2 schemes. We employ Model 1 to simulate the settling of a tridisperse ($N = 3$) suspension forming a compressible sediment [3]. The mixture is described by the model functions (3.2)–(3.4) with $\phi_{\max} = 0.66$, $n_{\mathrm{RZ}} = 4.7$, $\sigma_0 = 180\,\mathrm{Pa}$, $\phi_{\mathrm{c}} = 0.2$, $k = 2$, $\mu_{\mathrm{f}} = 10^{-3}\,\mathrm{Pa\,s}$, $d = 1.19 \times 10^{-5}\,\mathrm{m}$, $\bar{\rho}_{\mathrm{s}} = 1800\,\mathrm{kg/m^3}$, and $g = 9.81\,\mathrm{m/s^2}$. The initial concentration is $\Phi_0 = (0.04, 0.04, 0.04)^{\mathrm{T}}$ in a vessel of height $\mathcal{L} = 1\,\mathrm{m}$ with normalized squared particle sizes $\boldsymbol{\delta} = (1, 0.5, 0.25)^{\mathrm{T}}$. Here and in Examples 2 to 5 we employ the zero-flux boundary conditions (3.1).

Numerical results at simulated time $T = 4000\,\mathrm{s}$ are obtained by four schemes, i.e., LI-SSP-LDIRK(3,3,2) (see Figure 2), LI-H-LDIRK2(2,2,2), LI-H-LDIRK3(2,2,2), and LI-H-DIRK2(2,2,2), and are compared with those generated by their NI counterparts and the KT scheme. For the nonlinearly implicit schemes, we solve the nonlinear system by Algorithm 4.1 of [10] that uses a variant of the NR method with a prescribed relative tolerance tol, where the regularization $\boldsymbol{B}_\varepsilon$ of the original diffusion matrix $\boldsymbol{B}$ is

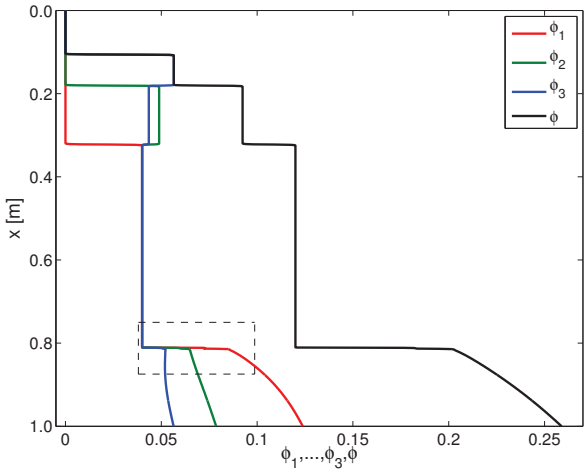

FIG. 2. *Example* 1 *(Model* 1*): Numerical solution obtained by scheme LI-SSP-LDIRK*(3,3,2) *at simulated time* $T = 4000\,\mathrm{s}$ *and* $\Delta x = 1/1600$.

achieved by replacing the function σ_e in (3.3) by $\sigma_e(\phi;\varepsilon) = \sigma_e(\phi)\exp(-\varepsilon/(\phi-\phi_c)^2)$, where $\varepsilon > 0$ decreases gradually from $\varepsilon_0 = 10^{-4}$ to $\varepsilon_{\min} = 10^{-6}$, $\mathrm{tol} = 10^{-8}$, while the linearly implicit and KT schemes are applied without regularization of the diffusive term (this also includes the reference solution). Another strategy, denoted by LI-SSP-LDIRK(2,2,2)-reg, is to use the scheme LI-SSP-LDIRK(2,2,2) directly applied to the regularized diffusion term with $\varepsilon_{\min} = 10^{-6}$. The schemes LI-H-LDIRK2(2,2,2)-reg, LI-H-LDIRK3(2,2,2)-reg, and LI-H-DIRK2(2,2,2)-reg are defined analogously. For both NI and LI versions of IMEX-RK schemes we use $C_{\mathrm{cfl}_2} = 0.7$, and for the KT scheme, $C_{\mathrm{cfl}_1} = 0.25$. Figures 3(a) and (b) provide the error histories of all schemes tested, and Figures 3(c) and (d) are the corresponding efficiency plots (informing approximate L^1 errors versus CPU time).

Figures 3(a) and (b) show that for all schemes tested and all discretizations, the error produced by linearly implicit schemes for a given discretization is larger than that of the corresponding nonlinear counterpart (as expected). Furthermore, for some of the schemes and some discretizations the "LI-reg" version of a scheme produces smaller errors than the corresponding linearly implicit version. This holds, for example, for schemes LI-H-DIRK3(2,2,2) and LI-DIRK2(2,2,2) for $M = 100$ and $M = 200$, as can be seen in Figure 3(b). However, there is no appreciable difference in the numerical order of accuracy of all schemes tested.

Figures 3(c) and (d) illustrate that although linearly implicit schemes produce larger errors than corresponding nonlinearly implicit schemes, they are still competitive since they are at least as efficient, and in many cases significantly more efficient, in error reduction per CPU time than their corresponding nonlinear counterparts (this is particularly visible if one compares the performance of the scheme NI-H-LDIRK3(2,2,2) with that of its linear counterpart; see Figure 3(d)). In fact, linearly implicit schemes have been designed to execute faster than their respective nonlinear counterparts, since the former need to solve only one linear system per RK stage, whereas the latter have to solve many during the nonlinear solves in Algorithm 4.1 of [10].

It is natural to expect that differences in solution behavior between the various

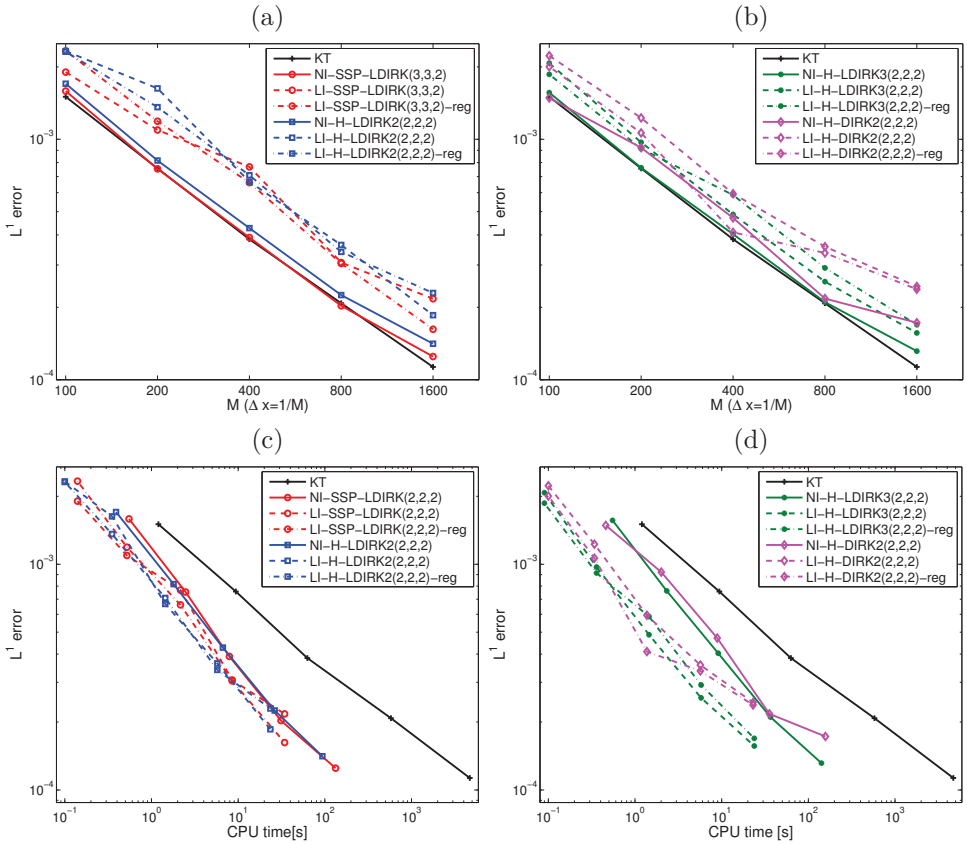

FIG. 3. *Example* 1 *(Model* 1*):* (a), (b) *Approximate* L^1 *errors for all schemes tested as function of* M*.* (c), (d) *Efficiency plots obtained for discretization levels* $\Delta x = 1/M$ *with* $M = 100$*,* 200*,* 400*,* 800*, and* 1600*.*

schemes become apparent close to the parabolic-hyperbolic interface $\phi = \phi_c$. To illustrate them, we present in Figure 4 enlarged views of the box area marked in Figure 2. As can be seen in all plots, the approximation of discontinuous solution profiles is more accurate for the nonlinearly implicit version of each scheme, while some overshoots and oscillations appear in the corresponding linearly implicit versions. These glitches do not disappear upon refinement. Therefore, the approximate errors with respect to the reference solution (computed without ε regularization) are larger for the linearly implicit versions than for the nonlinearly implicit versions, as is shown in Figures 3(a) and (b). The overshoots are especially pronounced with the scheme LI-H-LDIRK2(2,2,2) in Figure 4(a). At the same time we see that in this situation the corresponding "LI-reg" versions of each linearly implicit scheme produce slightly more accurate and less oscillatory solutions that their original linearly implicit versions.

4.3. Examples 2–4: Model 1 with $N = 3$, variation of $\varepsilon_{\min}$. Examples 2 to 5 are based on the same data as Example 1, but we now apply four schemes, namely, LI-SSP-LDIRK(3,3,2), LI-H-LDIRK2(2,2,2) (both with the SSP property), and their respective NI versions, to the ε-regularized problems with decreasing values of ε. The linearly implicit schemes keep solving one linear system per RK stage, whereas the nonlinearly implicit schemes need several of them and may need the gradual

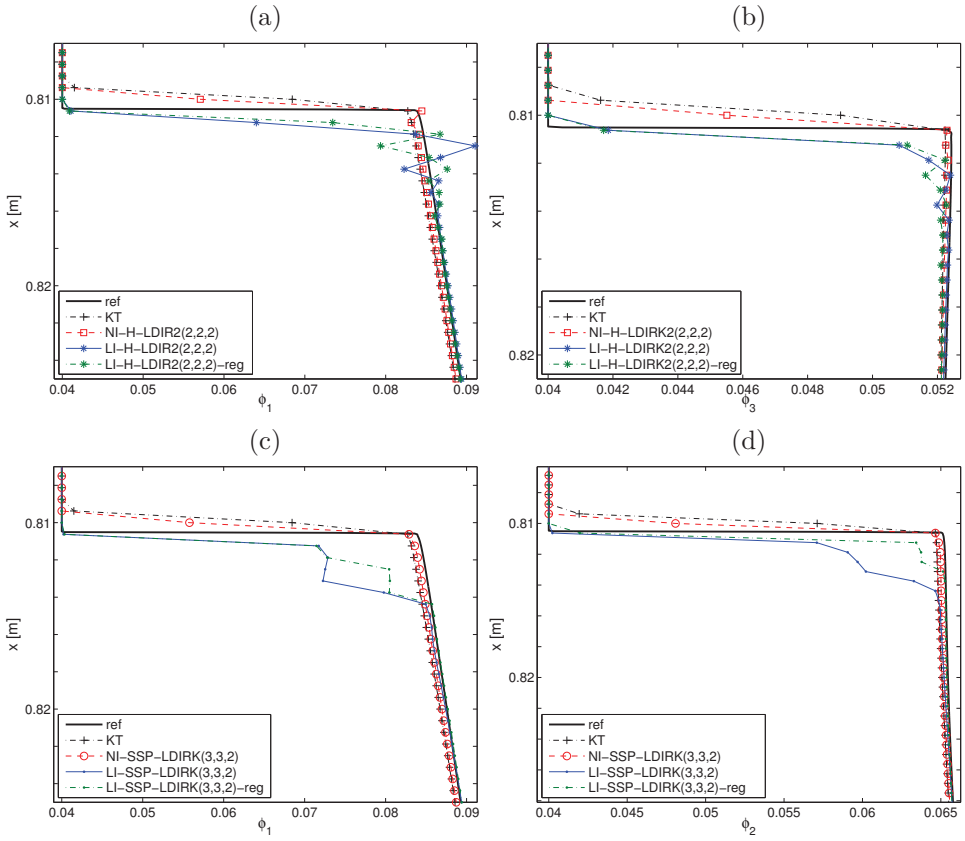

FIG. 4. *Example* 1 *(Model* 1*): Enlarged views of the numerical solution near the parabolic-hyperbolic interface* $\phi = \phi_c$ *(marked region in Figure* 2*).*

decrease of ε toward $\varepsilon_{\min}$. The reference solution is computed in each example to an ε-regularized diffusive term. Here we focus on studying the effect of varying $\varepsilon_{\min}$.

In Example 2, we choose a regularized diffusive term with $\varepsilon_{\min} = 10^{-3}$. In the results displayed in Figures 5(a)–(c), which are enlarged views of the results for each component corresponding to the marked region of Figure 2 of Example 1, we observe that the numerical solutions obtained with the linearly implicit schemes do not present overshoots. Moreover, Figure 5(d) shows that—at least for moderately fine discretizations—the linearly implicit schemes are slightly more efficient than their nonlinear counterparts.

Next, in Example 3, we choose the same parameters as in Examples 1 and 2 but regularize the diffusive term by $\varepsilon_{\min} = 5 \times 10^{-5}$. This regularization yields diffusion coefficients that are less smooth than in the previous example. Figure 6 shows the solutions that are analogous to Figure 5 for Example 2. In fact, the solutions displayed in Figures 6(a)–(c) are qualitatively similar, and the efficiency curves in Figure 6(d) of both linearly implicit schemes are closer to those of the corresponding nonlinearly implicit schemes.

Finally, in Example 4 we set $\varepsilon_{\min} = 5 \times 10^{-6}$. In the results displayed in Figures 7(a)–(c) we observe some glitches in the numerical solutions obtained with both linearly implicit schemes. Figure 7(d) indicates that the linearly implicit schemes are

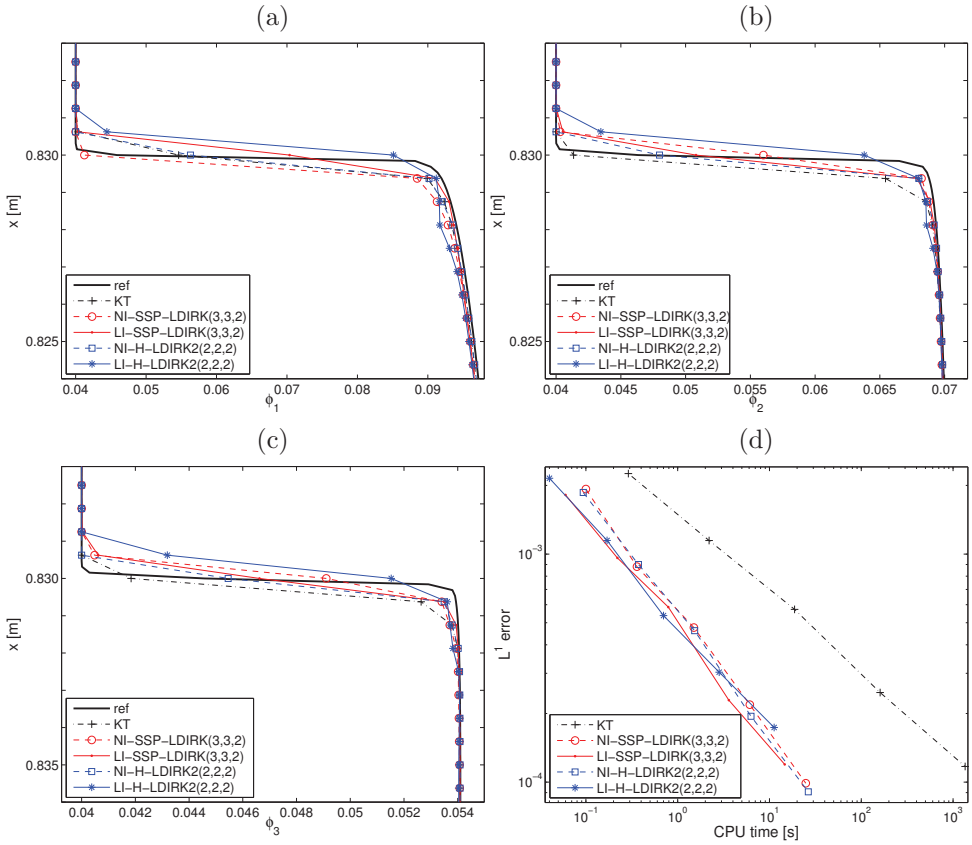

FIG. 5. *Example* 2 *(Model* 1*,* $N = 3$*, diffusive term regularized with* $\sigma_e(\phi; 10^{-3})$*):* (a)–(c) *Enlarged views of the numerical solution near the parabolic-hyperbolic interface* ($\phi = \phi_c$)*.* (d) *Efficiency plot for discretization levels* $\Delta x = 1/M$ *with* $M = 100$*,* 200*,* 400*,* 800*, and* 1600*.*

slightly more efficient than their respective nonlinear counterparts.

4.4. Example 5: Model 1 with $N = 3$, numerical order of accuracy. In this test we check the order of accuracy of the linearly implicit numerical schemes introduced in section 2.5 applied to the regularized model with $\varepsilon_{\min} = 0.1$. We consider the normalized squared particle sizes $\boldsymbol{\delta} = (1, 0.8, 0.6)^{\mathrm{T}}$ and a smooth initial concentration profile given by $\phi_i(x) = 0.12\exp(-200(x - 0.5)^2)$ for $i = 1, \ldots, 3$. We compute approximations with $M = 50 \cdot 2^l$, $l = 0, \ldots, 6$, and a fixed time step $\Delta t = 500\Delta x$, which yields a Courant number of 0.1. Figure 8 shows the numerical result for $M = 1600$ for $T = 20\,\mathrm{s}$ (before shock formation, when the solution is still smooth) and for $T = 500\,\mathrm{s}$ (after shock formation).

The approximate L^1 errors $e_M^{\mathrm{tot}}(T)$ defined by (4.1) and their corresponding numerical orders $\theta_M(T)$ given by (4.2) are displayed in Table 2 for both $T = 20\,\mathrm{s}$ and $T = 500\,\mathrm{s}$. The reference solution is computed with $M_{\mathrm{ref}} = 25600$ cells. We select the results for $T = 20\,\mathrm{s}$ to conduct an alternative error analysis (according to section 4.1). To this end we compute values of $\tilde{e}_M^{\mathrm{tot}}(20)$ according to (4.3), (4.4), (4.7), and the corresponding numerical orders of convergence $\hat{\theta}_M(20)$ given by (4.5). The behavior of both $\theta_M(20)$ and $\hat{\theta}_M(20)$ for increasing values of M confirms that the

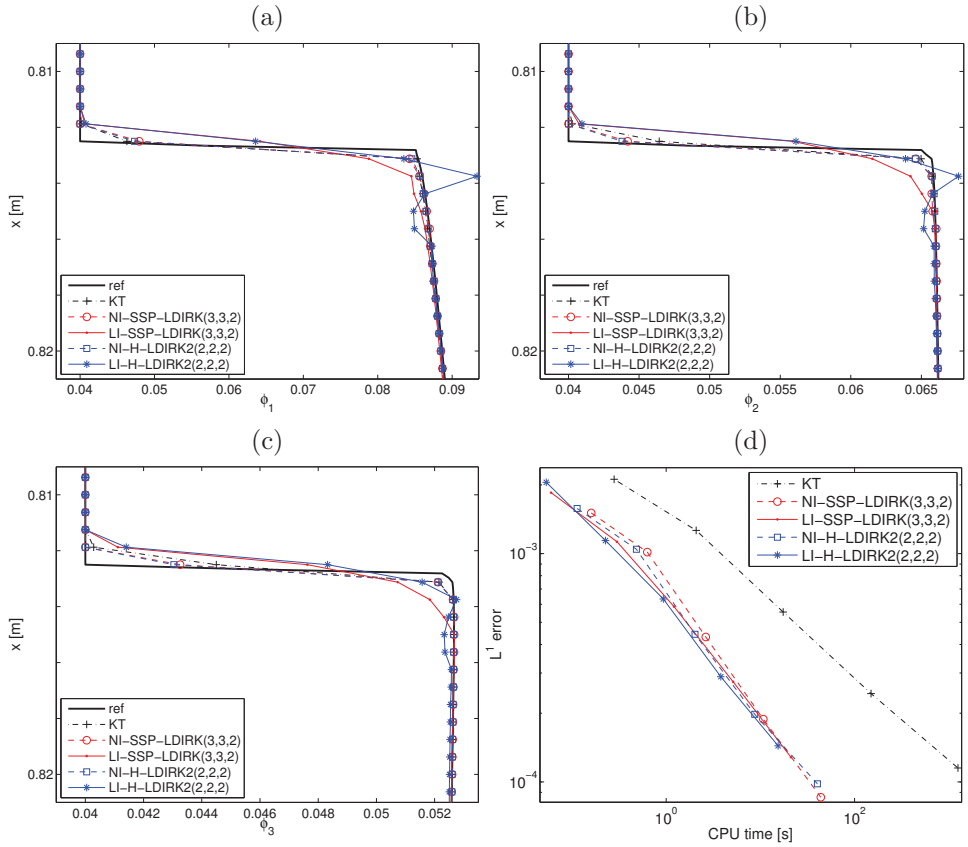

FIG. 6. *Example* 3 *(Model* 1*,* $N = 3$*, diffusive term regularized with* $\sigma_e(\phi; 5\times10^{-5})$*):* (a)–(c) *Enlarged views of the numerical solution near the parabolic-hyperbolic interface* ($\phi = \phi_c$)*.* (d) *Efficiency plot for discretization levels* $\Delta x = 1/M$ *with* $M = 100$*,* 200*,* 400*,* 800*, and* 1600*.*

scheme is second-order accurate for smooth solutions and that, for large M, the values of $\tilde{e}_M^{\mathrm{tot}}(20)$ are very close to those of the approximate L^1 errors $e_M^{\mathrm{tot}}(20)$, while the results for $T = 500\,\mathrm{s}$ indicate that accuracy is reduced to first order when shocks are present.

4.5. Example 6 (Model 2 with $N = 3$). We consider a circular road of length $K = 5\,\mathrm{mi}$ (mi stands for miles, and periodic boundary conditions (3.6) are used) with $N = 3$ driver classes associated with $v_1^{\max} = 70\,\mathrm{mi/h}$, $v_2^{\max} = 50\,\mathrm{mi/h}$, and $v_3^{\max} = 30\,\mathrm{mi/h}$. We employ the Dick–Greenberg model (3.8) and choose (as in [10]) $\phi_c = \exp(-7/\mathrm{e}) \approx 0.076142$. We choose $L = 0.05\,\mathrm{mi}$ and $\tau = 2\,\mathrm{s} = 0.000\bar{5}\,\mathrm{h}$, such that a particular sufficient condition for parabolicity of (1.1) for $\phi > \phi_c$ is satisfied.

The initial density distribution is given by an isolated platoon of maximum global density ρ_0, $\Phi_0(x,0) = p(x-0.3)\rho_0(0.25, 0.4, 0.35)^{\mathrm{T}}$, where $\rho_0 = 0.45$ and

$$p(x) = \begin{cases} 10x & \text{for } 0 \le x \le 0.1, \\ 1 & \text{for } 0.1 < x \le 0.9, \\ -10(x-1) & \text{for } 0.9 < x \le 1. \end{cases}$$

The nonlinear systems arising in the nonlinearly implicit schemes are solved by Al-

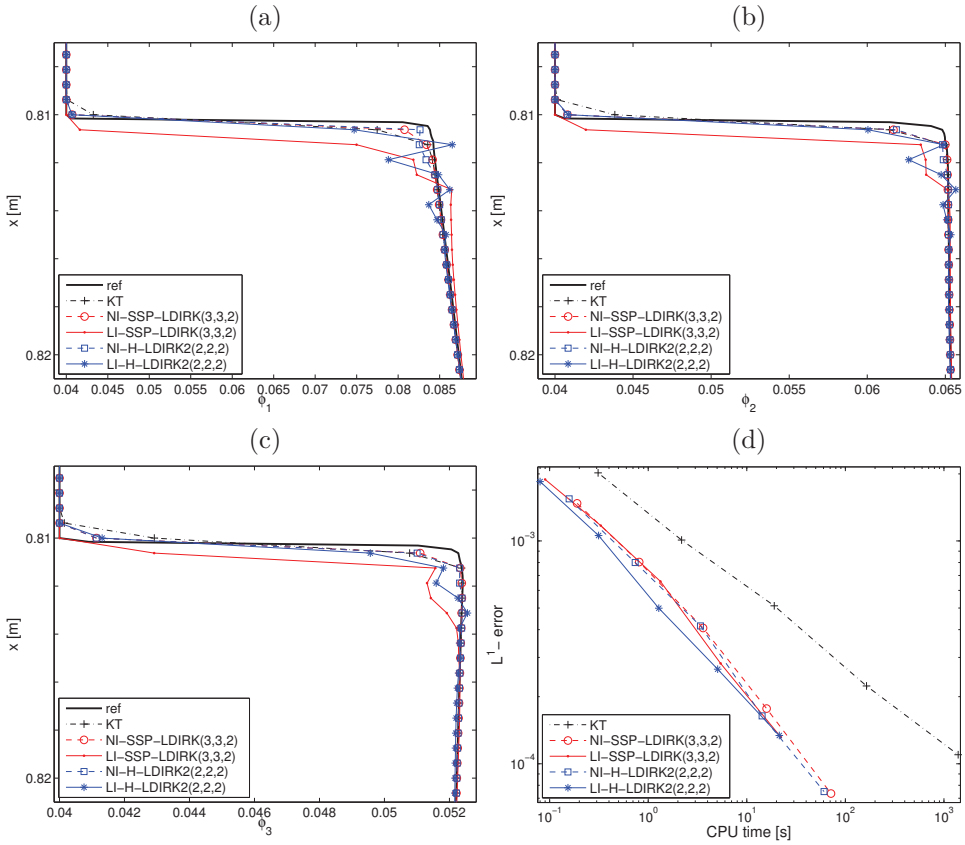

FIG. 7. *Example* 4 *(Model* 1*,* $N = 3$*, diffusive term regularized with* $\sigma_e(\phi; 5\times10^{-6})$*):* (a)–(c) *Enlarged views of the numerical solution near the parabolic-hyperbolic interface* ($\phi = \phi_c$). (d) *Efficiency plot for discretization levels* $\Delta x = 1/M$ *with* $M = 100$*,* 200*,* 400*,* 800*, and* 1600.

gorithm 4.1 of [10], where $V(\phi)$ is regularized by $V(\phi;\varepsilon) = 1+(V(\phi)-1)\exp(-\varepsilon/(\phi-\phi_c)^2)$, where ε varies from $\varepsilon_0 = 10^{-4}$ to $\varepsilon_{\min} = 10^{-6}$ and $\mathrm{tol} = 10^{-7}$.

The reference solution is computed by the KT scheme (without regularization) with $\Delta x = 1/6400$ and $C_{\mathrm{CFL}_2} = 0.25$.

In Figure 9(a) we display the numerical solution obtained by scheme LI-SSP-LDIRK(3,3,2) (without regularization) with $\Delta x = 1/400$ and $C_{\mathrm{CFL}_2} = 0.7$ at simulated time $T = 0.05\,\mathrm{h}$. Enlarged views are shown in Figures 9(b)–(f), where we compare the numerical solutions (at the same resolution) produced by the schemes NI-SSP-LDIRK(3,3,2), LI-H-LDIRK2(2,2,2), and LI-H-LDIRK3(2,2,2) and their NI counterparts with $C_{\mathrm{CFL}_2} = 0.7$, those generated by the KT and LI/NI-H-CN(2,2,2) schemes with $C_{\mathrm{CFL}_1} = 0.25$, and the reference solution. We observe that the approximation obtained by the scheme LI-SSP-LDIRK(3,3,2) adequately approximates the reference solution. In Figures 10(a) and (b) we display error and efficiency plots, respectively, for a sequence of discretization levels and all schemes tested. Roughly speaking, the results confirm the tendency observed in Figure 3 for Model 1: for a fixed discretization, each linearly implicit scheme produces a slightly larger error but executes significantly faster than its nonlinear counterpart, such that the linearly implicit schemes turn out to be notably more efficient than their corresponding nonlinear counterparts.

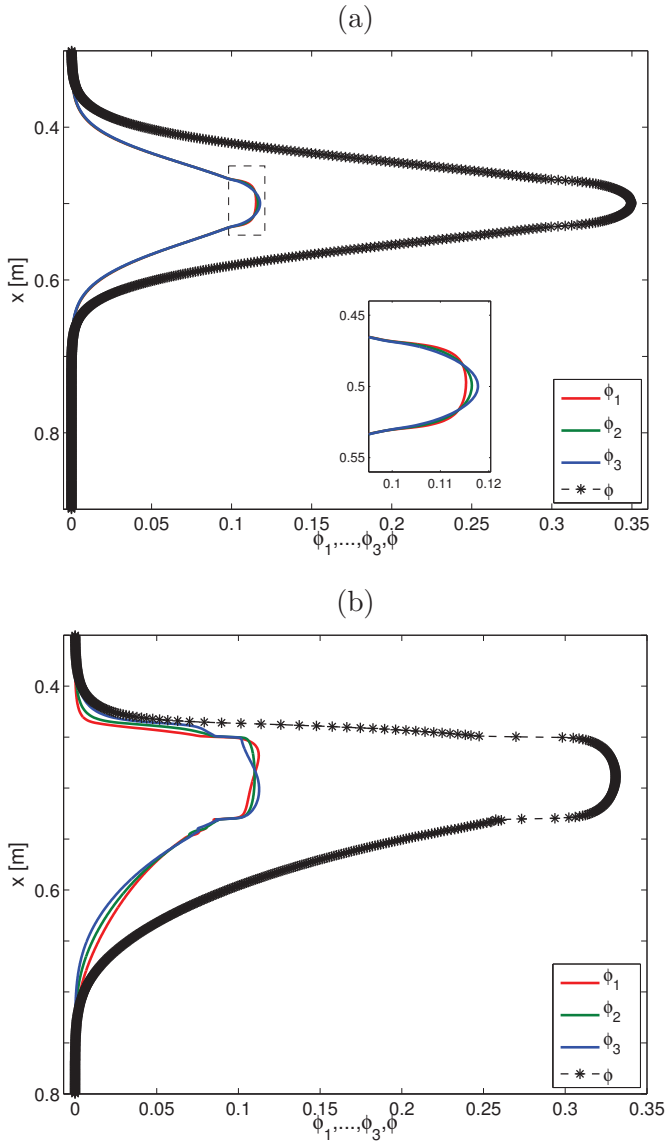

FIG. 8. *Example* 5 *(Model* 1, $N = 3$*): Numerical results obtained by scheme LI-SSP-LDIRK*(3,3,2)*-reg with* $M = 1600$ *at simulated time* (a) $T = 20\,\mathrm{s}$, (b) $T = 500\,\mathrm{s}$.

5. Concluding remarks. Although LI-IMEX-RK schemes might seem like a simple variant of NI-IMEX-RK schemes, they indeed suppose a profound change of paradigm for which the variables that bring stiffness to the explicit schemes are finely located in such a way that (a) at each RK stage only one linear system is solved, instead of a costly nonlinear solve that involves many of them; and (b) no accuracy order is lost.

The numerical examples presented herein indicate, first of all, that the new LI-IMEX-RK schemes yield very similar results, independently of the choice of the underlying RK schemes, that they approximate the same solutions as their nonlinear

TABLE 2

Example 5 *(Model* 1*,* $N = 3$*): Errors and numerical order for linearly implicit schemes applied to smooth initial conditions for* $T = 20\,\mathrm{s}$ *(before shock formation) and* $T = 500\,\mathrm{s}$ *(after shock formation).*

		$T = 20\,\mathrm{s}$				$T = 500\,\mathrm{s}$	
	M	$e_M^{\mathrm{tot}}(T)$	$\theta_M(T)$	$\tilde{e}_M^{\mathrm{tot}}(T)$	$\hat{\theta}_M(T)$	$e_M^{\mathrm{tot}}(T)$	$\theta_M(T)$
LI-SSP-LDIRK(3,3,2)	50	1.38e-4	0.14	8.41e-5	-0.33	2.27e-3	1.59
	100	1.25e-4	1.45	1.06e-4	1.48	7.49e-4	0.95
	200	4.58e-5	1.80	3.80e-5	1.68	3.86e-4	1.11
	400	1.30e-5	1.88	1.19e-5	1.76	1.78e-4	0.91
	800	3.54e-6	1.87	3.52e-6	1.87	9.49e-5	1.05
	1600	9.66e-7	2.00	9.63e-7	1.98	4.56e-5	1.01
	3200	2.40e-7	2.06	2.44e-7	—	2.26e-5	1.01
	6400	5.73e-8	—	—	—	1.12e-5	—
LI-H-LDIRK2(2,2,2)	50	1.38e-4	0.14	8.44e-5	-0.33	2.27e-3	1.60
	100	1.25e-4	1.45	1.06e-4	1.48	7.46e-4	0.95
	200	4.57e-5	1.81	3.79e-5	1.68	3.85e-4	1.11
	400	1.30e-5	1.89	1.18e-5	1.76	1.78e-4	0.91
	800	3.53e-6	1.87	3.51e-6	1.87	9.48e-5	1.05
	1600	9.64e-7	2.00	9.60e-7	1.98	4.56e-5	1.01
	3200	2.40e-7	2.07	2.43e-7	—	2.26e-5	1.72
	6400	5.71e-8	—	—	—	6.82e-6	—
LI-H-LDIRK3(3,3,2)	50	1.38e-4	0.14	8.45e-5	-0.32	2.27e-3	1.60
	100	1.25e-4	1.45	1.06e-4	1.48	7.46e-4	0.95
	200	4.57e-5	1.81	3.80e-5	1.68	3.85e-4	1.11
	400	1.30e-5	1.87	1.18e-5	1.76	1.78e-4	0.91
	800	3.53e-6	1.87	3.50e-6	1.87	9.49e-5	1.05
	1600	9.64e-7	2.01	9.60e-7	1.99	4.56e-5	1.01
	3200	2.40e-7	2.07	2.43e-7	—	2.26e-5	1.73
	6400	5.75e-8	—	—	—	6.82e-6	—
LI-H-DIRK2(2,2,2)	50	1.38e-4	0.14	8.42e-5	-0.33	2.27e-3	1.60
	100	1.25e-4	1.45	1.06e-4	1.48	7.46e-4	0.95
	200	4.58e-5	1.81	3.80e-5	1.68	3.85e-4	1.11
	400	1.31e-5	1.89	1.19e-5	1.77	1.78e-4	0.91
	800	3.53e-6	1.87	3.51e-6	1.87	9.48e-5	1.05
	1600	9.64e-7	2.01	9.61e-7	1.98	4.56e-5	1.01
	3200	2.40e-7	2.07	2.43e-7	—	2.26e-5	1.73
	6400	5.72e-8	—	—	—	6.82e-6	—
LI-H-CN(2,2,2)	50	1.38e-4	0.14	8.40e-5	-0.34	2.27e-3	1.60
	100	1.25e-4	1.45	1.06e-4	1.48	7.47e-4	0.95
	200	4.59e-5	1.81	3.80e-5	1.68	3.85e-4	1.11
	400	1.31e-5	1.89	1.19e-5	1.76	1.78e-4	0.91
	800	3.54e-6	1.87	3.51e-6	1.87	9.48e-5	1.06
	1600	9.65e-7	2.01	9.61e-7	1.98	4.56e-5	1.01
	3200	2.40e-7	2.07	2.43e-7	—	2.26e-5	1.73
	6400	5.73e-8	—	—	—	6.82e-6	—

counterparts (introduced in [10]), and that in many cases they are more efficient. In the case of the regularized problem with $\varepsilon_{\min} = 10^{-3}$ of Example 2, shown in Figure 5, the new linearly implicit schemes provide essentially the same results as the classical implicit IMEX at a much lower cost. The decisive advantage of the linearly implicit variant is the ease of implementation. While the numerical examples presented herein have been limited to $N = 3$ for the sake of presentation, this advantage is likely to

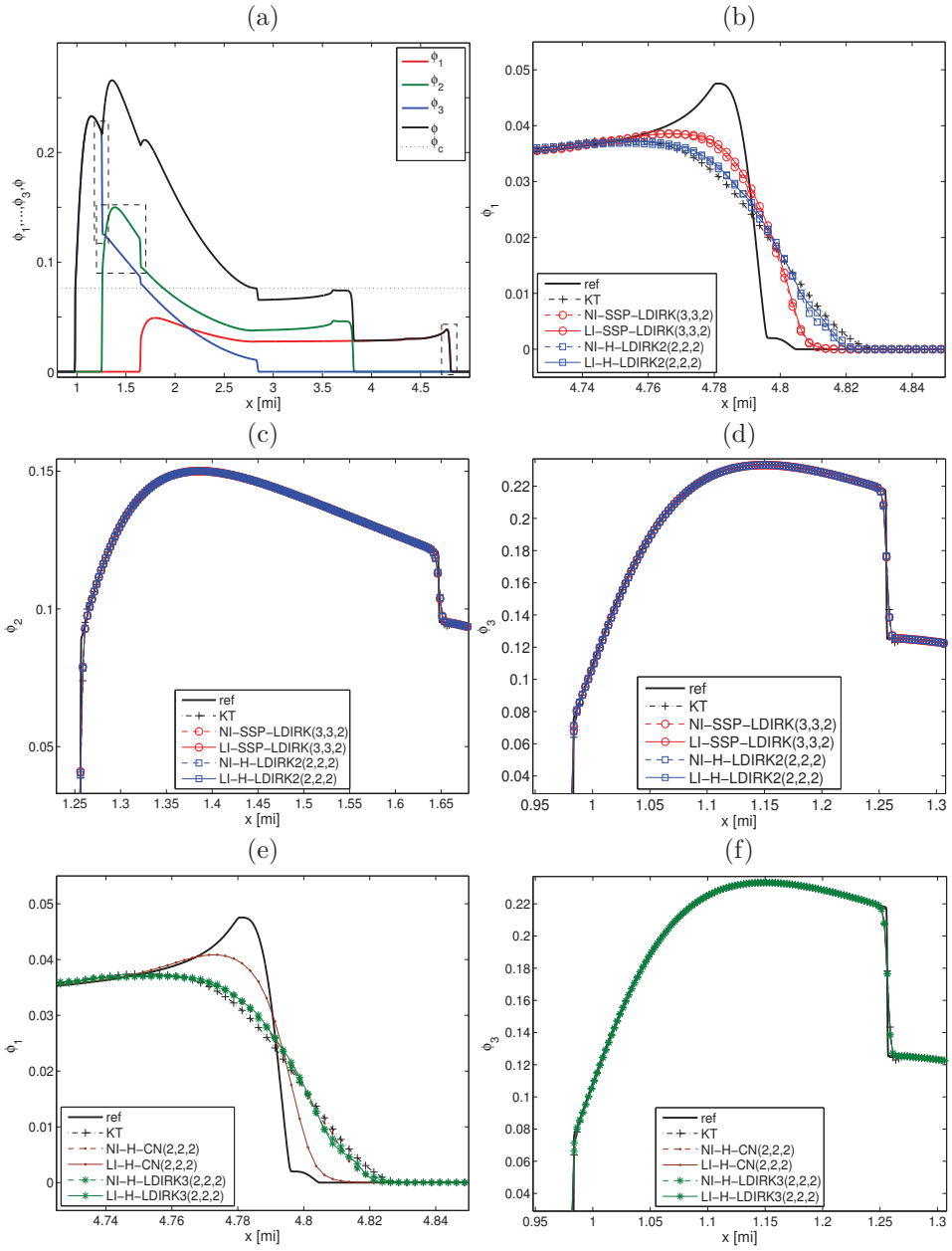

FIG. 9. *Example* 6 *(Model* 2, $N = 3$*): Numerical results at simulated time* $T = 0.05\,\mathrm{h}$ (a) *obtained by scheme LI-SSP-LDIRK*(3,3,2) *with* $\Delta x = 1/800$, (b)–(f) *obtained by other schemes and compared with the reference solution.*

become more stringent for larger values of N—for example, when in the context of the polydisperse sedimentation model (and related applications), a continuous particle size distribution is approximated by N size classes.

Both LI-IMEX-RK and NI-IMEX-RK schemes converge to the same solutions as the KT scheme does [22], which provides justification of their application, although

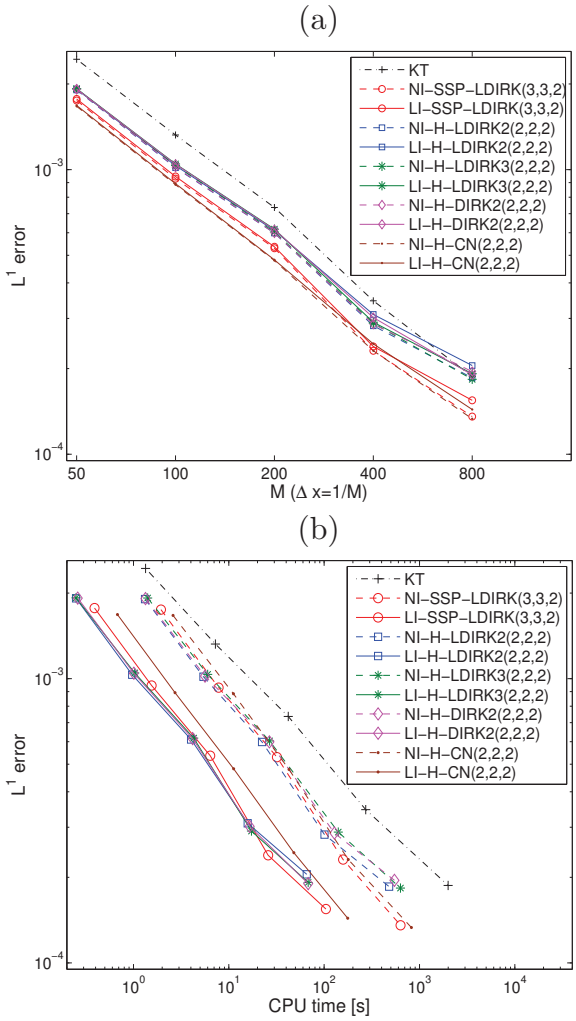

FIG. 10. *Example* 6 *(Model* 2, $N = 3$*): Efficiency plot based on numerical solutions for* $\Delta x = 1/M$ *with* $M = 50$, 100, 200, 400, *and* 800.

a well-posedness theory for (1.1), at least in the strongly degenerate case, is still lacking. However, it turns out that at the same spatial resolution, discontinuities in the solution, especially those associated with the type-change interface, are more accurately resolved by the NI-IMEX-RK schemes. It therefore seems highly desirable to combine the respective advantages of LI- and NI-IMEX-RK schemes by a hybrid scheme that would concentrate the use of the nonlinearly implicit variant on regions of presumed irregularities of the solution (such as discontinuities and kinks), which usually form only a small fraction of the computational domain, while in the remaining "smooth" regions the faster linearly implicit variant would be used. In other words, such a scheme would attain an accuracy similar to the nonlinear IMEX-RK one, at a computational cost almost the same as for the linearly implicit version.

The application to diffusively corrected kinematic flow models has been chosen as a test case for IMEX-RK schemes in [10] herein since this class of problems includes

systems (1.1) of arbitrary size N and provides meaningful justification for the assumption of strong degeneracy. On the other hand, the LI- and NI-IMEX-RK schemes do not involve the particular algebraic structure of these models, and could therefore also be applied to other models that can be cast in the form (1.1). In that context we recall that the WENO reconstruction is based on the computation of smoothness indicators that monitor the presence of irregularities in the solution. We are currently investigating the option of using the same smoothness indicators to design a hybrid scheme of the above-mentioned kind.

Appendix A. Assume that the computed approximations $\phi_{j,i}^M(t)$ satisfy

$$\phi_{j,i}^M(t) = \phi_i(x_j,t) + a_i(x_j,t)\Delta x^r + \mathcal{O}(\Delta x^{r+1}), \tag{A.1}$$

where $\Delta x = \mathcal{L}/M$ and $x_j = (j-1/2)\Delta x$, for $r \le 2$ and sufficiently smooth coefficient functions a_j. Then it can be seen that the quantities defined by (4.3) satisfy

$$\tilde{\phi}_{j,i}^M(t) = \phi_i(x_j,t) + a_i(x_i,t)(\Delta x/2)^r + \mathcal{O}(\Delta x^{r+1}). \tag{A.2}$$

We recall that we calculate an alternative (with respect to (4.1)) total approximate L^1 error from the quantities (4.3) by (4.4), and that the (unknown) exact total error $e_M^{\mathrm{tot},*}(t)$ is given by (4.6). From (A.1), (A.2), and standard quadrature rules, we get

$$\hat{e}_M^{\mathrm{tot}}(t) = a(t)(1-2^{-r})\Delta x^r + \mathcal{O}(\Delta x^{r+1}), \quad a(t) = \sum_{i=1}^{N} \int \left|a_i(x,t)\right| \mathrm{d}x,$$

and $e_M^{\mathrm{tot},*}(t) = a(t)\Delta x^r + \mathcal{O}(\Delta x^{r+1})$. We therefore deduce that

$$\lim_{M\to\infty} \left(\hat{e}_M^{\mathrm{tot}}(t)/\hat{e}_{2M}^{\mathrm{tot}}(t)\right) = 2^r \quad \text{and} \quad \lim_{M\to\infty} \left(\hat{e}_M^{\mathrm{tot}}(t)/e_M^{\mathrm{tot},*}(t)\right) = 1-2^{-r},$$

i.e., for the quantity $\hat{\theta}_M(t)$ given by (4.5) we have $\hat{\theta}_M(t) \to r$ as $M \to \infty$, and for large M the exact total error $e_M^{\mathrm{tot},*}(t)$ can be estimated from $\hat{e}_M^{\mathrm{tot}}(t)$ by

$$e_M^{\mathrm{tot},*}(t) \approx \tilde{e}_M^{\mathrm{tot}}(t) := (1-2^{-r})^{-1}\hat{e}_M^{\mathrm{tot}}(t),$$

which yields (4.7) for $r = 2$.

Appendix B. We prove that the stability region S_1 of scheme H-DIRK2(2,2,2) coincides with that of the classical Heun scheme, while the stability region S_1 of scheme H-CN(2,2,2) coincides with that of the explicit Euler scheme. Such results are not obvious. In particular, the first one is interesting, since the choice of an A-stable scheme for the implicit part provides a wider stability region S_1 than the choice of the more stable LDIRK schemes for the implicit part.

THEOREM B.1. *The stability region*

$$S_1 = \left\{ z_1 \in \mathbb{C} : \sup_{z\in\mathbb{C}^-} |R(z_1,z)| \le 1 \right\}$$

*of the H-DIRK*2(2,2,2) *scheme coincides with the stability region of the Heun scheme*

$$S_H = \left\{ z_1 \in \mathbb{C}^- \, : \, \left| 1 + z_1 + \frac{z_1^2}{2} \right| \le 1 \right\}.$$

Proof. For this method, we employ the matrices $\tilde{\boldsymbol{A}}$ and $\boldsymbol{A}$ and the vector $\boldsymbol{b}^{\mathrm{T}}$ given in Table 1(b). Evaluating (2.15) in Lemma 2.1 then yields that

$$R(z_1, z) = \left(1 + z_1 + \frac{z_1^2}{2} - \frac{z^2}{4}\right) \Big/ \left(1 - \frac{z}{2}\right)^2.$$

We have that $R(z_1, z)$ is bounded and analytic in $\mathbb{C}^-$ with respect to z since

$$\lim_{|z|\to\infty} \big|R(z_1, z)\big| = 1,$$

and the only singularity of R is in $z = 2$.

The maximum principle for analytic functions implies that

$$\sup_{z\in\mathbb{C}^-} \big|R(z_1, z)\big| = \sup_{z\in\partial\mathbb{C}^-} \big|R(z_1, z)\big| = \sup_{\zeta\in\mathbb{R}} \big|R(z_1, 2\mathrm{i}\zeta)\big|. \tag{B.1}$$

Now setting $z_1 = x + \mathrm{i}y$, $z = 2\mathrm{i}\zeta$ and defining $C = x + (x^2 - y^2)/2$, $B = y(x + y)$, we get

$$1 + z_1 + \frac{z_1^2}{2} = 1 + C + B\mathrm{i}, \quad 1 + z_1 + \frac{z_1^2}{2} - \frac{z^2}{4} = 1 + C + \zeta^2 + B\mathrm{i}$$

and therefore

$$\big|R(z_1, z)\big|^2 = \frac{(1 + C + \zeta^2)^2 + B^2}{(1 + \zeta^2)^2} = 1 + \frac{2C(1 + \zeta^2) + C^2 + B^2}{(1 + \zeta^2)^2},$$

so $|R(z_1, z)|^2 \le 1$ if and only if $2C(1+\zeta^2)+C^2+B^2 \le 0$. Thus $\sup_{\zeta\in\mathbb{R}} |R(z_1, 2\mathrm{i}\zeta)| \le 1$ if and only if $2C + C^2 + B^2 \le 0$, or, equivalently,

$$\left|1 + z_1 + \frac{z_1^2}{2}\right|^2 = (C + 1)^2 + B^2 \le 1. \qquad \square$$

THEOREM B.2. *The stability region S_1 of the Heun-CN(2,2,2) scheme coincides with the stability region of explicit Euler scheme*

$$S_E = \big\{z_1 \in \mathbb{C}^- \,:\, |1 + z_1| \le 1\big\}.$$

Proof. The proof is similar to that of Theorem B.1. For this method, we utilize $\tilde{\boldsymbol{A}}$, $\boldsymbol{A}$, and $\boldsymbol{b}^{\mathrm{T}}$ as given in Table 1(a). Evaluating (2.15) in Lemma 2.1, we now obtain

$$R(z_1, z) = \left(1 + z_1 + z_1^2 + \frac{z}{2}(1 + z_1)\right) \Big/ \left(1 - \frac{z}{2}\right).$$

Since $\lim_{|z|\to\infty} |R(z_1, z)| = |1 + z_1|$, we have that $R(z_1, z)$ is bounded and analytic in $\mathbb{C}^-$ with respect to z. The maximum principle for analytic functions yields that (B.1) is again valid. Setting now $z_1 = x + \mathrm{i}y$, $z = 2\mathrm{i}\zeta$, and $C := x + (x^2 - y^2)/2$, we get

$$1 + z_1 + \frac{z_1^2}{2} = 1 + C + y(x + 1)\mathrm{i}, \quad \frac{z}{2}(1 + z_1) = \zeta(-y + (1 + x)\mathrm{i}),$$

and finally

$$\big|R(z_1, z)\big|^2 = \frac{(1 + C - y\zeta)^2 + (y + \zeta)^2(1 + x)^2}{1 + \zeta^2}.$$

This implies that $|R(z_1, z)|^2 \leq 1$ is equivalent to

$$\zeta(\zeta + y)((1+x)^2 + y^2 - 1) + (1+C)^2 + y^2(1+x)^2 - 1 \leq 0. \tag{B.2}$$

Since $1 + C = \frac{1}{2}((x+1)^2 + 1 - y^2)$,

$$(1+C)^2 + y^2(1+x)^2 = \frac{1}{4}\Big(((x+1)^2 + y^2 + 1)^2 - 4y^2\Big). \tag{B.3}$$

Setting $D := (1+x)^2 + y^2 - 1 = |z_1 + 1|^2 - 1$, then (B.3) reads as

$$(1+C)^2 + y^2(1+x)^2 = \frac{1}{4}\Big((D+2)^2 - 4y^2\Big)$$

and (B.2) as

$$D\zeta^2 + Dy\zeta + \frac{1}{4}(D^2 + 4D - 4y^2) \leq 0. \tag{B.4}$$

Therefore we have established the equivalence of $|R(z_1, 2\mathrm{i}\zeta)|^2 \leq 1$ for all $\zeta \in \mathbb{R}$ and (B.4) holding for any $\zeta \in \mathbb{R}$. This is in turn equivalent to

$$D \leq 0 \quad \text{and} \quad D(D+4)(y^2 - D) \leq 0. \tag{B.5}$$

However, since $D \geq -1$, we have $D + 4 > 0$, and therefore $D \leq 0$ implies $D(D + 4)(y^2 - D) \leq 0$, which yields that (B.5) is equivalent to $D \leq 0$, which is precisely equivalent to $|1 + z_1| \leq 1$, thus concluding the proof. □

REFERENCES

[1] U. Ascher, S. Ruuth, and J. Spiteri, *Implicit-explicit Runge-Kutta methods for time dependent partial differential equations*, Appl. Numer. Math., 25 (1997), pp. 151–167.

[2] S. Benzoni-Gavage and R.M. Colombo, *An n-populations model for traffic flow*, European J. Appl. Math., 14 (2003), pp. 587–612.

[3] S. Berres, R. Bürger, K.H. Karlsen, and E.M. Tory, *Strongly degenerate parabolic-hyperbolic systems modeling polydisperse sedimentation with compression*, SIAM J. Appl. Math., 64 (2003), pp. 41–80.

[4] S. Boscarino, F. Filbet and G. Russo, *High order semi-implicit schemes for time dependent partial differential equations*, submitted for publication.

[5] S. Boscarino, P.G. LeFloch, and G. Russo, *High-order asymptotic-preserving methods for fully nonlinear relaxation problems*, SIAM J. Sci. Comput., 36 (2014), pp. A377–A395.

[6] S. Boscarino, L. Pareschi, and G. Russo, *Implicit-explicit Runge–Kutta schemes for hyperbolic systems and kinetic equations in the diffusion limit*, SIAM J. Sci. Comput., 35 (2013), pp. A22–A51.

[7] S. Boscarino and G. Russo, *On a class of uniformly accurate IMEX Runge–Kutta schemes and applications to hyperbolic systems with relaxation*, SIAM J. Sci. Comput., 31 (2009), pp. 1926–1945.

[8] S. Boscarino and G. Russo, *Flux-explicit IMEX Runge–Kutta schemes for hyperbolic to parabolic relaxation problems*, SIAM J. Numer. Anal., 51 (2013), pp. 163–190.

[9] R. Bürger, R. Donat, P. Mulet, and C.A. Vega, *On the implementation of WENO schemes for a class of polydisperse sedimentation models*, J. Comput. Phys., 230 (2011), pp. 2322–2344.

[10] R. Bürger, P. Mulet, and L.M. Villada, *Regularized nonlinear solvers for IMEX methods applied to diffusively corrected multispecies kinematic flow models*, SIAM J. Sci. Comput., 35 (2013), pp. B751–B777.

[11] J.E. Dennis, Jr., and R.B. Schnabel, *Numerical Methods for Unconstrained Optimization and Nonlinear Equations*, Classics Appl. Math. 16, SIAM, Philadelphia, 1996.

[12] R. Donat and P. Mulet, *Characteristic-based schemes for multi-class Lighthill-Whitham-Richards traffic models*, J. Sci. Comput., 37 (2008), pp. 233–250.

[13] J. Frank, W. Hundsdorfer, and J.G. Verwer, *On the stability of implicit-explicit linear multistep methods*, Appl. Numer. Math., 25 (1997), pp. 193–205

[14] S. Gottlieb, C.-W. Shu, and E. Tadmor, *Strong stability-preserving high-order time discretization methods*, SIAM Rev., 43 (2001), pp. 89–112.

[15] M. Gunther and A. Sandu, *A Class of Generalized Additive Runge-Kutta Methods*, Technical Report CSL-TR-5/2013, Virginia Polytechnic Institute and State University Computational Science Laboratory, 2013.

[16] E. Hairer, S.P. Nørsett, and G. Wanner, *Solving Ordinary Differential Equations.* I. *Nonstiff Problems*, 2nd ed., Springer Ser. Comput. Math. 8, Springer-Verlag, Berlin, 1993.

[17] I. Higueras, N. Happenhofer, O. Koch, and F. Kupka, *Optimized IMEX Runge-Kutta Methods for Simulation in Astrophysics: A Detailed Study*, ASC Report 14/2012, Institute for Analysis and Scientific Computing, Vienna University of Technology, 2012

[18] W. Hundsdorfer and J.G. Verwer, *Numerical Solution of Time-Dependent Advection-Diffusion-Reaction Equations*, Springer-Verlag, Berlin, 2003.

[19] K.H. Karlsen and N.H. Risebro, *Convergence of finite difference schemes for viscous and inviscid conservation laws with rough coefficients*, M2AN Math. Model. Numer. Anal., 35 (2001), pp. 239–269.

[20] K.H. Karlsen and N.H. Risebro, *On the uniqueness and stability of entropy solutions of nonlinear degenerate parabolic equations with rough coefficients*, Discrete Contin. Dyn. Syst., 9 (2003), pp. 1081–1104.

[21] C.A. Kennedy and M.H. Carpenter, *Additive Runge-Kutta schemes for convection-diffusion-reaction equations*, Appl. Numer. Math., 44 (2003), pp. 139–181.

[22] A. Kurganov and E. Tadmor, *New high-resolution central schemes for nonlinear conservation laws and convection-diffusion equations*, J. Comput. Phys., 160 (2000), pp. 241–282.

[23] S.F. Liotta, V. Romano, and G. Russo, *Central schemes for balance laws of relaxation type*, SIAM J. Numer. Anal., 38 (2000) pp. 1337–1356

[24] J.M. Ortega and W.C. Rheinboldt, *Iterative Solution of Nonlinear Equations in Several Variables*, Classics Appl. Math. 30, SIAM, Philadelphia, 2000.

[25] L. Pareschi and G. Russo, *Implicit-Explicit Runge-Kutta schemes and applications to hyperbolic systems with relaxation*, J. Sci. Comput., 25 (2005), pp. 129–155.

[26] L. Pareschi and G. Russo, *Implicit-explicit Runge-Kutta schemes for stiff systems of differential equations*, in Recent Trends in Numerical Analysis, D. Trigiante, ed., Nova Science, Huntington, NY, 2001, pp. 269–288.

[27] P. Ullrich and C. Jablonowski, *Operator-split Runge-Kutta-Rosenbrock methods for nonhydrostatic atmospheric models*, Mon. Wea. Rev., 140 (2012), pp. 1257–1284.

[28] G.C.K. Wong and S.C. Wong, *A multi-class traffic flow model—an extension of LWR model with heterogeneous drivers*, Transp. Res. A, 36 (2002), pp. 827–841.

[29] X. Zhong, *Additive semi-implicit Runge-Kutta methods for computing high-speed nonequilibrium reactive flows*, J. Comput. Phys., 128 (1996), pp. 19–31.